UFL/COEL-74/033

HALOCLINE EROSION DUE TO WIND INDUCED STRESS

By

Kenneth K. Humiston

Thesis

1974

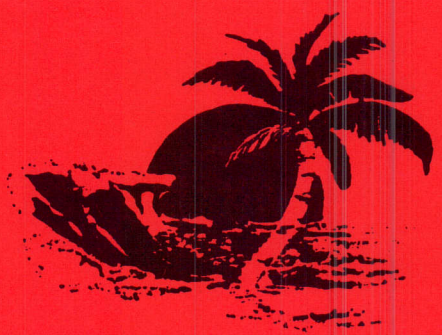

COASTAL & OCEANOGRAPHIC ENGINEERING DEPARTMENT

University of Florida • Gainesville, Florida 32611

HALOCLINE EROSION DUE TO WIND INDUCED STRESS

By

KENNETH K. HUMISTON

A THESIS PRESENTED TO THE GRADUATE COUNCIL OF
THE UNIVERSITY OF FLORIDA
IN PARTIAL FULFILLMENT OF THE REQUIREMENTS FOR THE
DEGREE OF MASTER OF ENGINEERING

UNIVERSITY OF FLORIDA

1974

ACKNOWLEDGEMENTS

I wish to thank Dr. Omar H. Shemdin, Chairman of my supervisory committee, for his encouragement and guidance in the preparation of this thesis, and for his part, as Director of the Coastal and Oceanographic Engineering Laboratory, in making the excellent internal wave facility there available for this study. I also extend my thanks to the other members of my supervisory committee, Dr. Robert G. Dean, Dr. D. Max Sheppard, and Dr. Yu-Hwa Wang for their instruction and inspiration during the period of my graduate learning and thesis preparation. Special thanks are due Dr. Wang and Dr. Ronald J. Lai for their assistance with the instrumentation during the experimental investigation. Finally a word of thanks to Tena Jones and Evelyn Hill for typing, Denise Frank for drafting, and the personnel at the Laboratory for their cooperation and assistance in obtaining and setting up the experimental apparatus.

TABLE OF CONTENTS

LIST OF FIGURES

LIST OF SYMBOLS

A - A constant

D - Depth

E(k) - Scalar energy

K - Curvature

N - Brunt-Väisälä Frequency

R_i - Richardson number

U - Velocity

a - A constant

b - Fluctuating component of buoyancy force

g - Gravity

i - Subscript, i = 1, 2, 3

k - Wave number

l - Length

ℓ - Mixing length

m - Unit vector upwards

n - Mixing frequency

p - Pressure

r - Separation vector

t - Time

U - Mean velocity

u' - Perturbation velocity

u_e - Entrainment velocity

u_* - Shear velocity

u_α - Horizontal velocity components

w - Vertical velocity fluctuations

ψ_{ij} - Velocity spectrum tensor

α - Subscript, $\alpha = 1, 2$

β - Angle between direction of velocity U and wave number k

ε - Viscous dissipation

ρ - Density

ρ_a - Density of air

ρ_w - Density of water

ρ_o - Reference density

τ - Shear stress

μ - Viscosity

μ_e - Eddy viscosity

Astract of Thesis Presented to the Graduate Council
of the University of Florida in Partial Fulfillment of the
Requirements for the Degree of Master of Engineering

Halocline Erosion Due to Wind Induced Stress

By

Kenneth K. Humiston

August, 1974

Chairman: Omar H. Shemdin
Major Department: Coastal Engineering

A laboratory investigation of the effects of wind on the depth of formation of a halocline is presented. A wave tank measuring 24.39 m long by 1.83 m high by 0.61 m wide was filled to a depth of 0.75 m with water so that a continuous density stratification was obtained, the varying density being achieved by varying salt concentrations. This stratified system was subjected to a wind induced stress at the surface and the changes in the velocity and density profiles and horizontal turbulent fluctuations were measured. It was found that on a macroscopic scale a discontinuous density jump initially forms below the surface a short time after the wind starts blowing, thereafter the interface is depressed by entrainment of the more dense lower layer in the turbulent upper layer. The rate of entrainment is dependent upon an overall Richardson number. Comparison of the horizontal turbulent energy spectra for stratified and unstratified situations shows a greater decreasing level of energy with depth in the presence of a stable stratification.

Omar H. Shemdin
Chairman

I. INTRODUCTION

A shear stress applied to a fluid boundary will induce motion and, if the Reynolds number is high enough, turbulence. In a fluid with a stable stratification the turbulent mixing results in the formation of a layer nearly homogeneous with respect to density. This layer extends from the surface of applied stress down to a level at which a discontinuous jump in density marks the border between the turbulent region and the underlying region where the original density distribution may remain unchanged. The extent of the homogeneous layer is dependent upon the magnitude and duration of the applied stress, physical parameters of the fluid, and characteristics of the flow. The formation of the discontinuous density jump inhibits further extension of the homogeneous layer by acting as a barrier to turbulent mixing.

This phenomenon is observed in many areas of significance and economic importance. Heavy atmospheric layers which form and are resistant to mixing may enhance air pollution problems. Methane can accumulate in high areas of a coal mine shaft where the extent of mixing with ventilating air has an important bearing on safety (Ellison and Turner, 1959). The degree of mixing of thermal discharges from water cooled power plants is important to the ecology of the surrounding area.

This thesis examines the formation of a discontinuous density jump in a stably stratified body of water when a wind induced shear stress

is applied to the surface. In the experiments conducted here the formation of a halocline is analagous to the formation of a thermocline in nature. Varying salinity was used to achieve density stratification rather than temperature since the latter is more difficult to control in the laboratory situation due to the high rate of thermal diffusion as compared to molecular diffusion. (Turner, 1968). Knowledge of the process involved will be useful in the study of internal waves as well as in situations such as quiescent basins and thermal discharges where a stable stratification may be altered by climactic conditions and form a barrier to vertical mixing.

The concept of entrainment is important in the process being studied. The turbulent region grows as the underlying non-turbulent region becomes entrained in it. The rate of entrainment can be described by an entrainment coefficient. Morton, Taylor, and Turner (1956) were the first to use such an entrainment coefficient in their examination of entrainment in buoyant plumes rising through a stably stratified ambient body of water. They found the entrainment constant to be proportional to the axial vertical velocity of the plume. Ellison and Turner (1959) performed a series of experiments on stratified flows induced by a heavy salt solution flowing down the sloping bottom beneath a layer of fresh water, and the spread of a surface jet of lighter fluid over a heavier ambient fluid. They measured a characteristic velocity at the interface by timing the movement of entrained sheets of fluid and found that the ratio of the entrainment velocity to the characteristic mean flow velocity is a function of a stability parameter having the form of a Richardson Number,

$$R_i = \frac{g(\rho - \rho_0)h}{\rho_0 V^2}$$

where V is the characteristic velocity, ρ is the density of the fluid,

g is the acceleration of gravity and h is the thickness of the turbulent layer and the subscript o refers to the reference fluid. Turner (1968) did some experiments on turbulent entrainment with no mean shear to determine the effects of molecular diffusivity. He found that it is not always possible to neglect molecular effects when the stability is high and the Reynolds number is not very large. By comparison of experiments using salinity to experiments using temperature to obtain stratification, he showed however, that below a critical value of the Richardson Number the entrainment is independent of diffusivity. This value is $R_i \cong 1$, where R_i is defined

$$R_i = \frac{g\Delta\rho}{\rho \ell n^2}$$

where n is the frequency of the mechanical mixing generating the turbulence $\Delta\rho$ is the difference between the densities of the turbulent and non-turbulent regions and ℓ is the mixing length. The results of these experiments also show an inverse proportionality between his Richardson number and entrainment velocity u_e, namely $u_e \alpha R_i^{-1}$. u_e is the rate of depression of the interface.

Kato and Phillips(1969) did an experiment in which they applied a constant shear stress to the surface of an annular tank containing water with a linear stratification. A motor in the center of the tank rotated an annular screen at the water surface, constant shear was obtained by mounting the motor on a bearing then restraining it from turning with a spring, and adjusting the controls so that the tension in the spring was constant. They observed that the mean velocity varied most rapidly near the surface below the screen and immediately above the interface which formed shortly after the constant shear was applied. The central region remained relatively uniform. When the interface reached the lower quarter

of the tank the density jump had become so large that entrainment virtually ceased, yet the fluid below the interface was set in motion by the purely viscous stress across it, the rate of diffusion of momentum by molecular viscosity being greater than that of salt by molecular diffusion.

The Reynolds number UD/ν, where U is the speed of the screen, D the depth of the layer and ν the kinematic viscosity, during these experiments ranged from 5×10^3 to 2×10^4, large enough, so that the large scale structure of the turbulence would be independent of the molecular viscosity. The properties of the turbulence are characterized by the friction velocity $u_* = \sqrt{\tau/\rho}$ and D. Their entrainment constant E defined as the ratio of the entrainment velocity u_e, to the friction velocity u_*, is thus a function of; the fractional change in buoyancy across the interface $g\frac{\delta\rho}{\rho_o}$ where ρ_o is the density of fresh water, the friction velocity itself, and the depth D of the interface, characterizing the scale of the turbulence. Grouping these three variables in a dimensionless group gives an overall Richardson number

$$R_{i_o} = \frac{g\ \delta\rho\ D}{\rho_o\ u_*^2} .$$

Furthermore, since the upper layer is nearly homogeneous, a salt balance computation gives

$$\delta\rho = \frac{1}{2} \left(\frac{\partial\rho}{\partial z}\right)_o D \quad ,$$

where $\left(\frac{\partial\rho}{\partial z}\right)_o$ is the initial density gradient, so that

$$R_{i_o} = \frac{g\left(\frac{\partial\rho}{\partial z}\right)_o D^2}{2\rho_o\ u_*^2} \quad .$$

Thus the entrainment coefficient is a function of the Richardson Number,

$$E = \frac{u_e}{u_*} = f(R_{i_o}) \quad .$$

Employing the same functional relationship as Turner, $u_e \alpha R_i^{-1}$, Kato and Philips proposed the empirical relationship

$$E = \frac{u_e}{u_*} = 2.5 \frac{\rho_o u_*^2}{g \delta\rho D} ,$$

where the numerical constant is stated to be uncertain to within 30 per cent.

II. THEORY

The mechanisms involved in halocline (or thermocline) erosion can be described in terms of the turbulent energy equation for horizontally homogeneous turbulence (see Phillips,1969)

$$\frac{\partial}{\partial t}\overline{u_i'^2} + \frac{\partial}{\partial t}\overline{\{w'(p/\rho_o + \frac{1}{2}u_i'^2)} = \overline{u'_\alpha w'}\frac{\partial U_\alpha}{z} + \overline{b'w'} - \varepsilon, \qquad (1)$$

where u_i' is the fluctuating component of the velocity, w' is the vertical fluctuating velocity, p is pressure, U is the mean velocity, b' is the fluctuating component of the buoyancy force and ε represents viscous dissipation. The subscript i = 1, 2, 3 and subscript α = 1, 2 specifying velocity components. The first term on the right is the rate of transfer of energy from the mean flow to turbulence by the work of the Reynolds stresses. The second term on the left represents the convective redistribution of turbulent energy in physical space by the turbulence itself. In the presence of a halocline some of the energy imparted to turbulence would be redistributed in the region of the interface where turbulent eddies entrain fluid from the more dense lower layer and mix it with the turbulent upper layer. This increases the density of the upper layer and therefore increases the potential energy of the mean buoyancy field. The transfer of kinetic to potential energy is represented by the covariance between the fluctuations in vertical velocity and buoyancy in Equation (1). The continued entrainment of fluid from the lower layer results in the erosion of the interface at a rate referred to earlier as the

entrainment velocity u_e. Referring again to the results of Kato and Phillips(1969), this entrainment velocity can be shown to be a function of an overall Richardson number characterizing the stability of the system.

Turbulence is frequently described in terms of spectral quantities. Phillips(1969, chapter 6) shows how the scalar energy spectrum, E(K),

$$E(K) = \frac{1}{2} \int \psi_{ii}(\vec{K})\, d\, S(K) \ , \qquad (2)$$

can be obtained from the velocity covariance tensor of the velocity field at a given instant, where $\psi_{ij}(\vec{K})$ is the wave number spectrum tensor or the Fourier transform of the covariance with respect to the separation vector between the two points under consideration. Philips then postulates that the energy density of turbulence is reduced in the presence of a stable stratification. This is a consequence of a reduction in the covariance between vertical velocity fluctuations which reduces the apparent eddy viscosity defined as

$$\mu_e(z) = A\, \rho \int \cos^2\beta\ \psi_{33}(\vec{K},\ \sigma=-\vec{K}\cdot\vec{U}(z),\ z)\ dk \ , \qquad (3)$$

where A is numerical constant and β is the angle between $\vec{K}$ and $\vec{U}$. This results in a reduction in the Reynolds stress gradient

$$\frac{d\tau}{dz} = \mu_e \frac{d^2U}{dz^2} \ , \qquad (4)$$

and the stress itself if $\tau = 0$ at some point in the flow, so for a given velocity gradient the energy flux $\tau\frac{dU}{dz}$ is also decreased. Since the energy flux is of the order u'^3/ℓ (Tennekes and Lumley, 1972) the energy density of the turbulence is also reduced, reducing the eddy viscosity still further.

For this postulate to be correct the turbulent energy spectrum in Eq. (2) should show a lower level in stratified flow when compared to the spectrum in an unstratified flow, all other conditions being equivalent.

For isotropic turbulence the longitudinal contribution to the total kinetic energy of the turbulence is just one third of that value, so that the above postulate could be verified with one dimensional velocity measurements. A major aim of the experimental study described here is to verify the postulate proposed above.

III. EXPERIMENTAL EQUIPMENT AND PROCEDURES

The experiments were conducted in the internal waves tank, 24 meters long by .6 meters wide and 1.22 meters high, with a wind section above the water .95 meters wide and .6 meters high (Figure 1). A complete description of the tank was given by Sheppard, Shemdin, and Wang (1973). The tank was initially filled to a level of 37.5 cm with fresh water, then filled slowly from the bottom with .02% salt water to bring the level to 75 cm. From this an approximately linear profile was obtained by dragging a board the length of the tank, at the interface between the salt and fresh water. The board was positioned perpendicular to the length of the tank and the interface, so that as it moved along the interface the turbulent eddies which formed behind the board caused mixing between the two layers. This process was continued until the desired degree of mixing was obtained.

The density profiles were measured initially with a single electrode conductivity probe (Gibson and Schwarz, 1963) but due to the low frequency drift, calibration was impossible, so the probes were modified by insertion of a length of tygon tubing into each probe so that samples of water could be siphoned from the wave tank at any level. The density could then be measured with a hydrometer to an accuracy of four decimal places, although the procedure is rather tedious.

Once the desired density profile was set, wind was produced by pulling air through the tank with an axial flow variable pitch fan, manufactured by Joy, and an integral part of the wave tank unit. Three fans settings were used over the course of the experimentation, corresponding to wind velocities of 2, 2.5, and 3 meters per second. Wind velocity profiles were

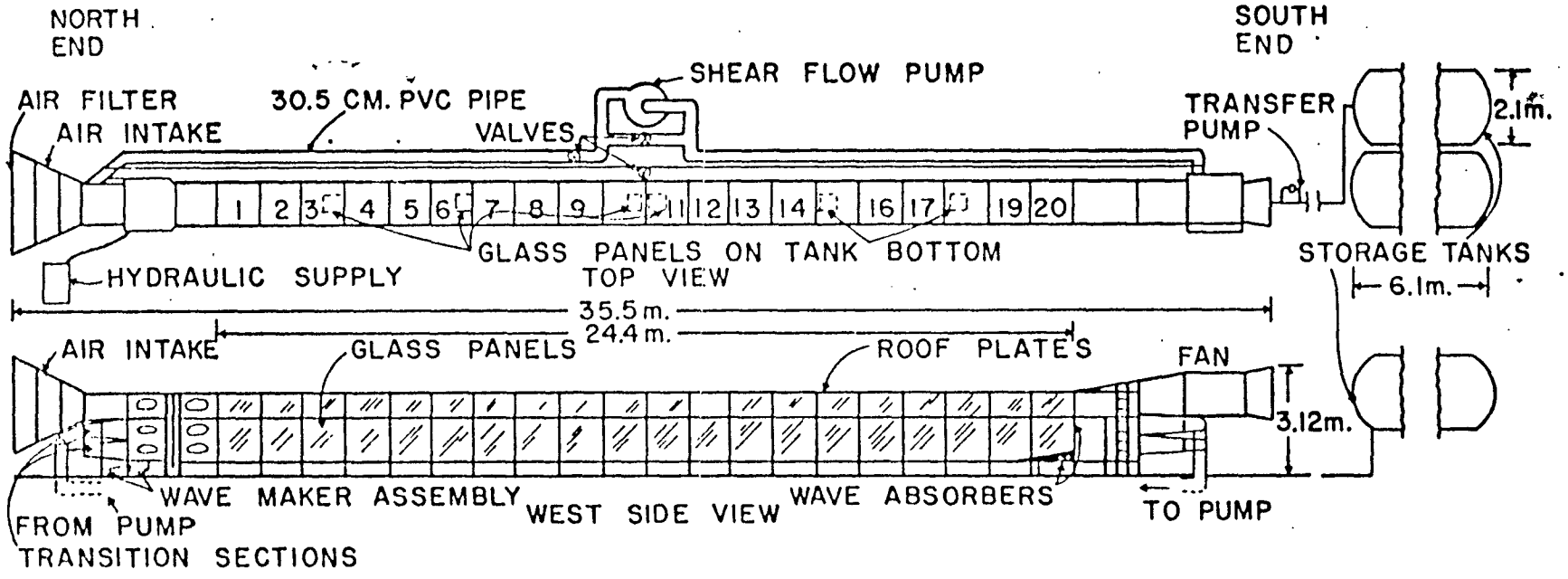

Fig. 1. Schematic drawing of the facility showing the overall dimensions and the location of the various components.

measured above the water surface with a pitot static tube, manufactured by United Sensor and Control Corp., a Pace Model P90D differential pressure transducer, a Disa Type 52B30 True Integrator signal conditioner and a Darcy Model 440 digital multimeter (Figure 2).

For each wind velocity, observations were made for wind durations of 3, 4, and 5 hours. In each case density profiles were measured before alteration by the wind, for the dynamic situation with the wind blowing, and after the wind was turned off allowing sufficient time for internal oscillations to die out. The tank was refilled after each run in an attempt to recreate the initial density structure as accurately as possible.

Velocity profiles were measured with hydrogen bubble wire and tracer dye, but these methods proved inadequate due to the fluctuating salinity. The hydrogen bubble wire failed because bubbles too large formed in regions of high salinity while regions of low salinity saw no bubbles at all. The tracer dye method was inadequate due to buoyancy effects.

Because of the failure of the velocity profile measurements, it was decided to run more experiments to obtain velocity profiles with a hot film anemometer system. A Thermo-systems, Inc. hot film sensor, model 1233 NACL was mounted on a vertical traverse mechanism anchored firmly at the top and bottom to reduce vibrations. The sensor was moved vertically with a pulley-cable setup. The anemometry system consisted of a Thermo-systems model 1051 power supply and indicator, and a model 1055 linearizer. The output was channeled simultaneously through the Disa integrator and Darcy DVM to obtain the mean voltage directly, and through a Thermo-systems correlator, model 1015C. The correlator amplified the signal by a factor of 10 to reduce any subsequent interference by noise when recorded on a Midwestern Instruments tape recorder. The recorded signal was analysed

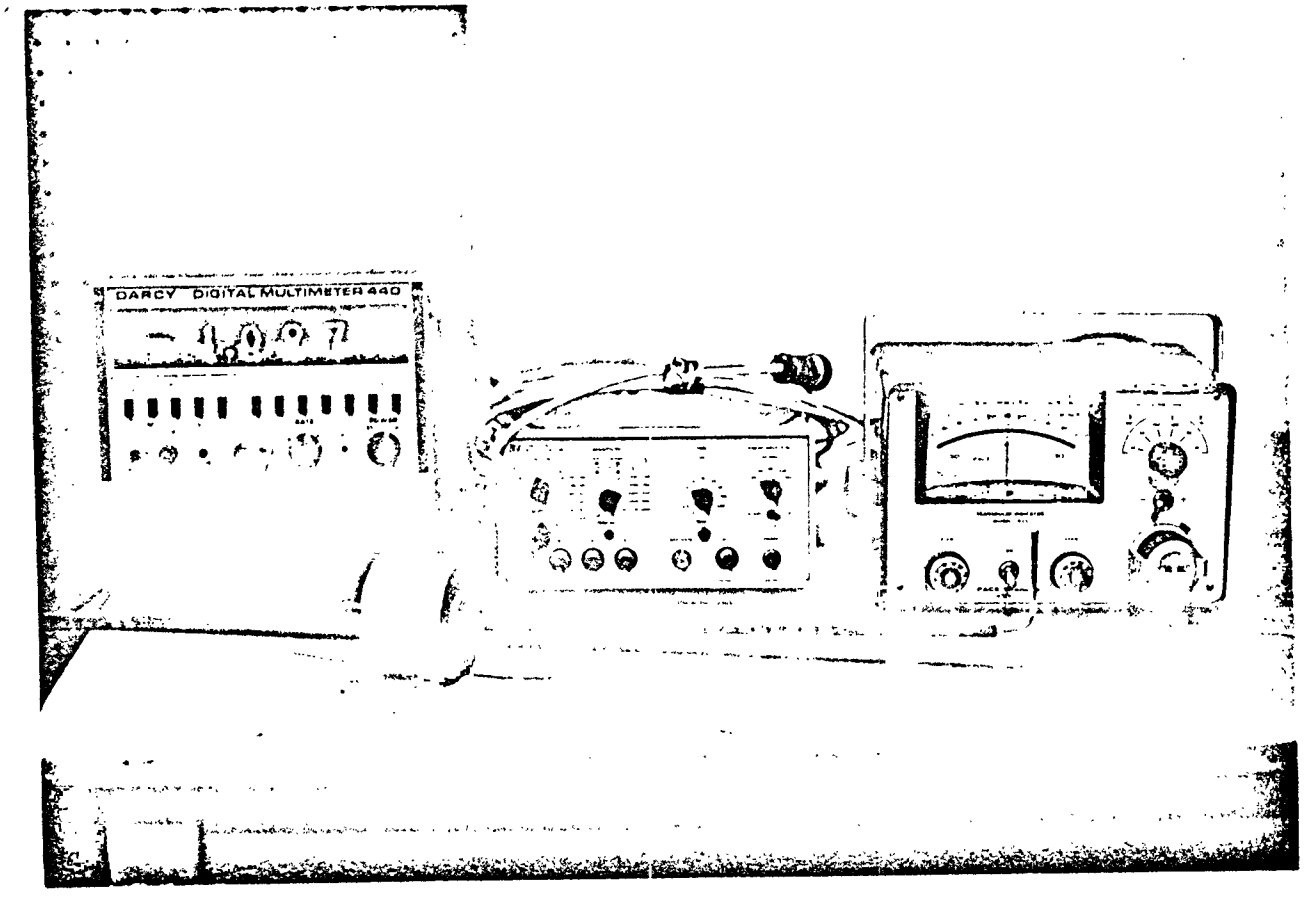

Figure 2. Wind velocity measurement instrumentation, pitot tube, pace transducer, signal conditioner and voltmeter.

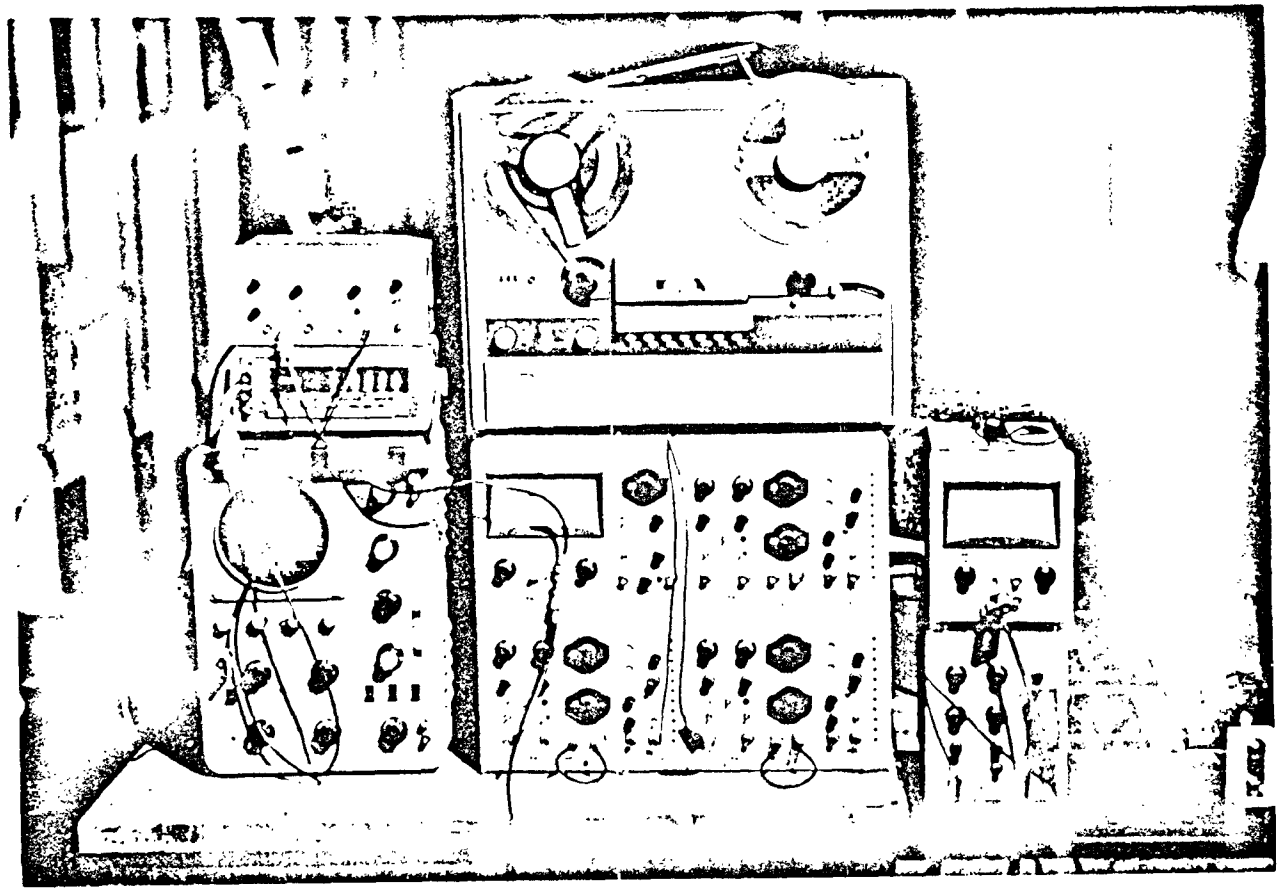

Figure 3. Hot-film anemometry instrumentation; anemometer power supply and linearizer, integrator, voltmeter, tape recorder, and rms meter.

on a Thermo-systems 1060 rms meter, and the Weston-Boonshaft and Fuchs series 711 spectrum analyser. Figure 3 shows the anemometry instrumentation.

Calibration of the velocity sensor was carried out in a plexiglass tow tank. Calibrations were done in water of different salinities in order to determine the dependence of response on salinity. Figure 4 shows the calibrations at various salinities. Bubbles sometimes formed on the tip of the sensor, probably due to disolved gases coming out of solution. It was found that the tendency for bubbles to form at the sensor tip increased with exposure time to the salt water, so immediately prior to the data taking run the overheat ratio was reduced and a calibration curve was obtained in water of specific gravity 1.0070, which is close to that expected in the top layer during a run. The calibration is displayed in Figures 5 and 6.

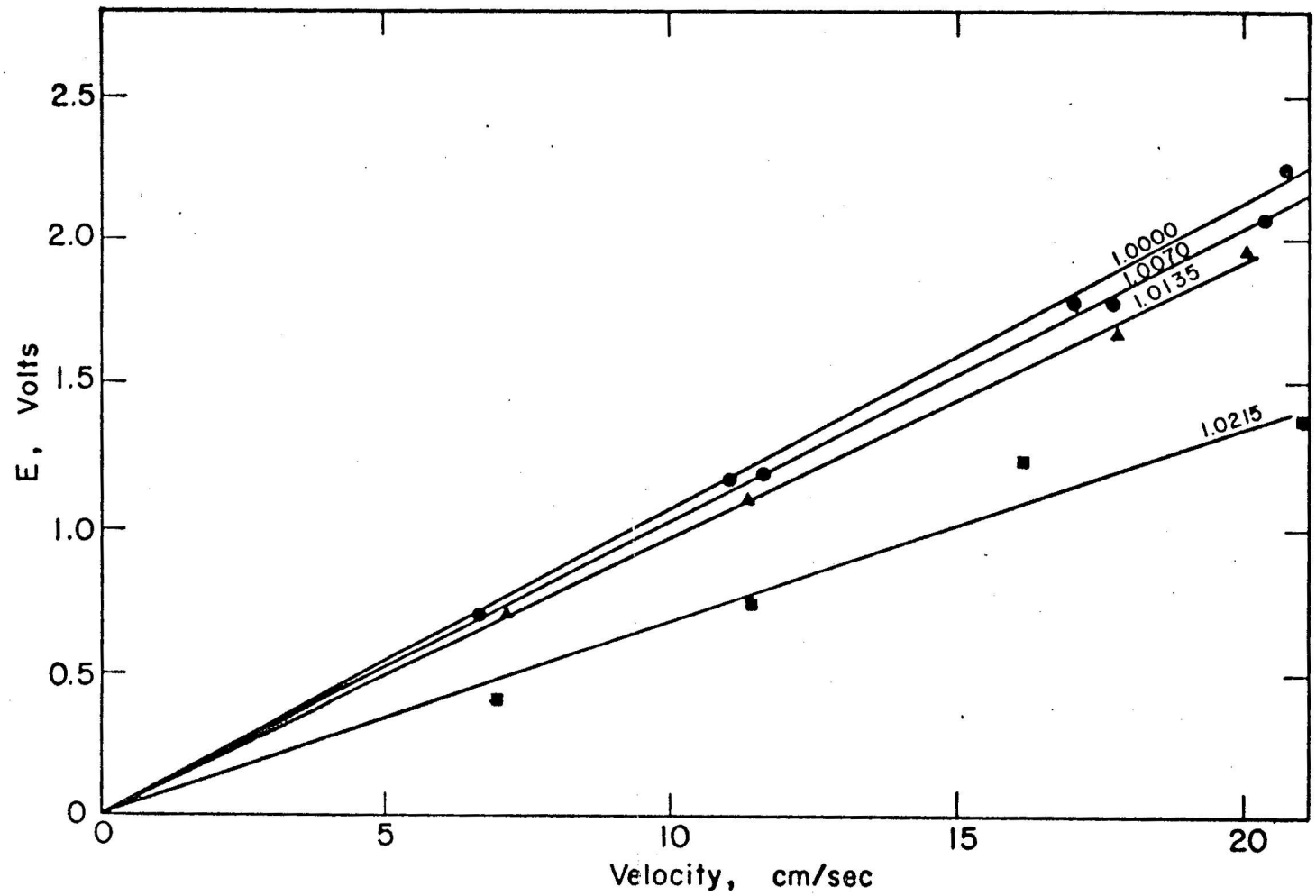

Figure 4. Hot film calibration by specific gravity, 0 - 21 cm/sec.

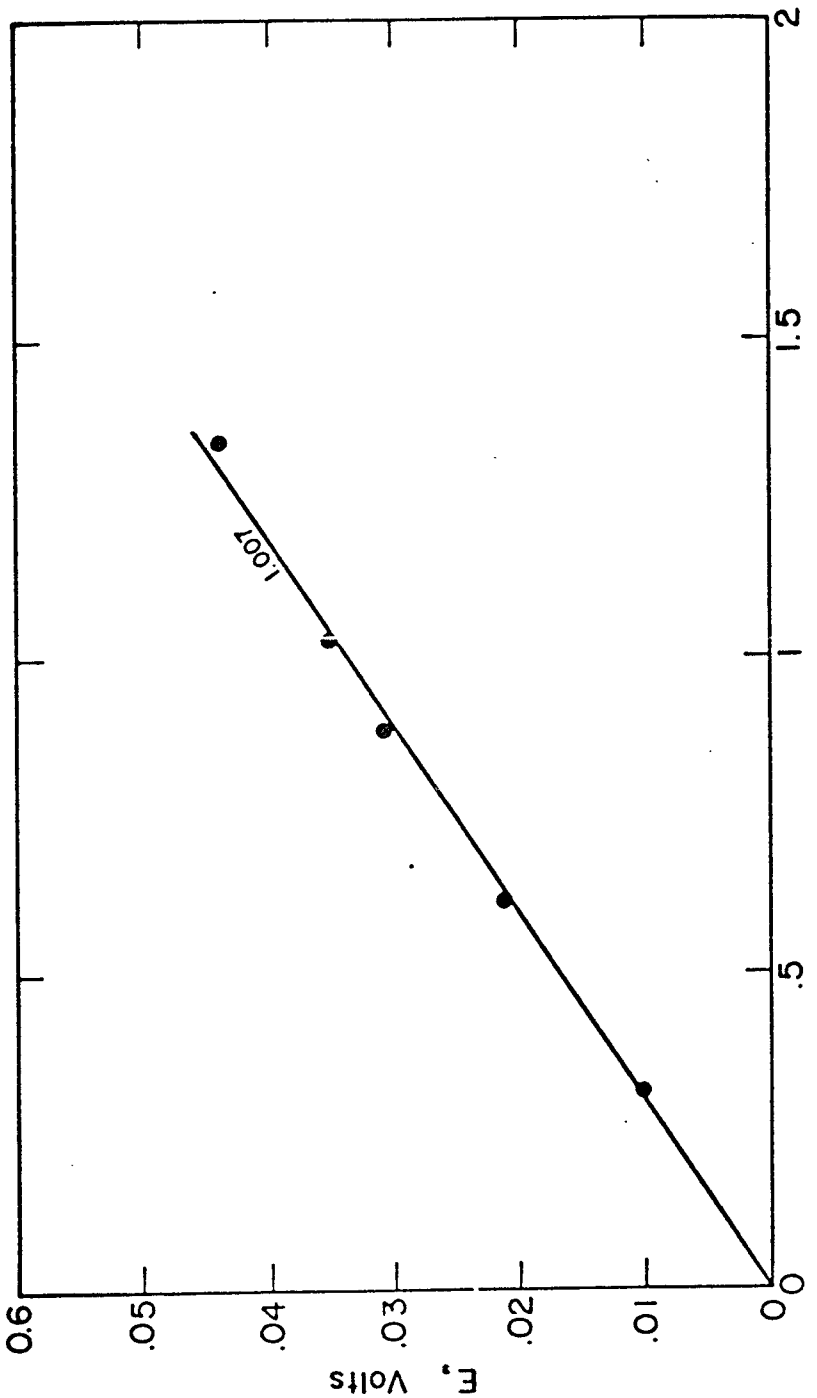

Figure 5. Hot film calibration by specific gravity, 0 - 1.5 cm/sec.

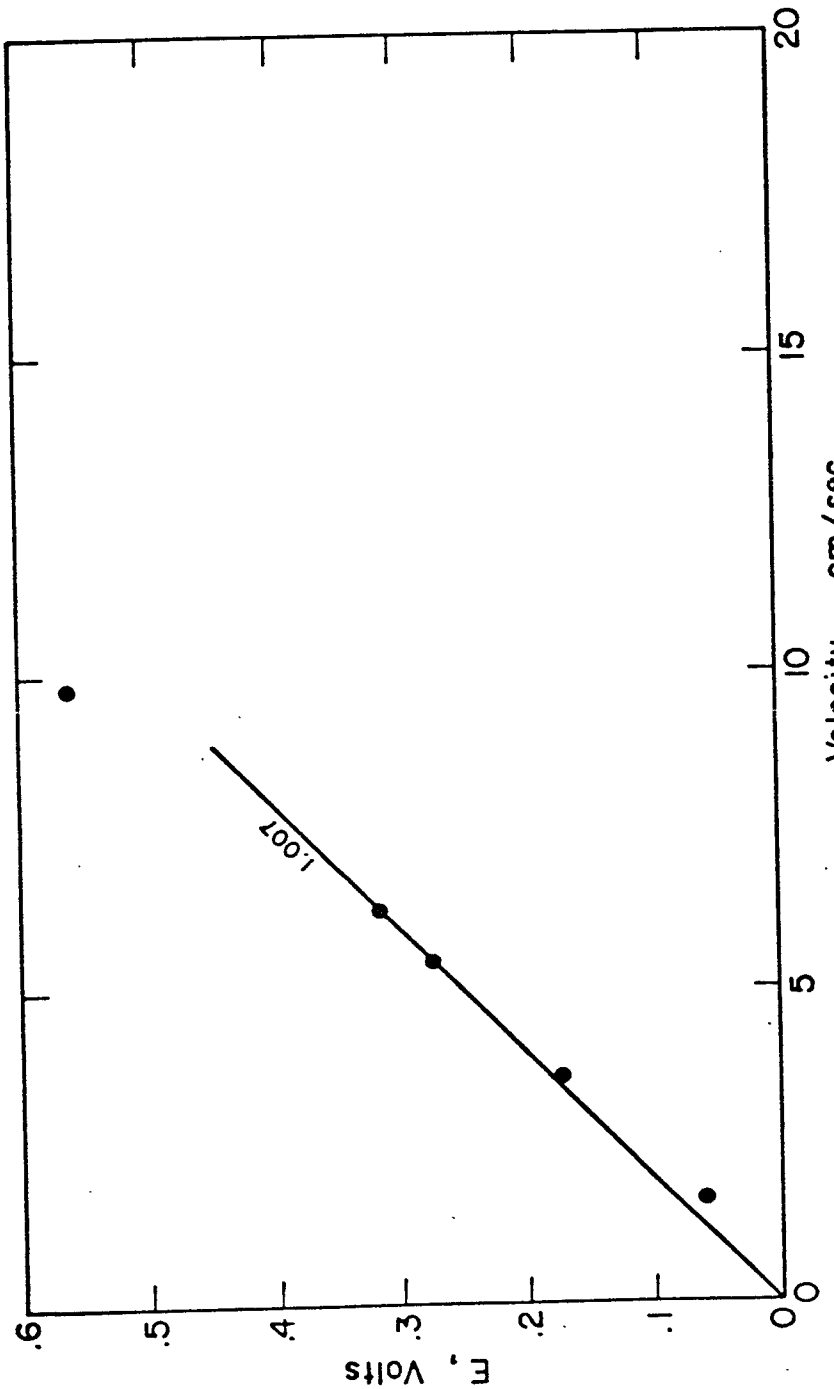

Figure 6. Hot film calibration by specific gravity, 0 - 10 cm/sec.

IV. RESULTS

The results presented are from two phases of experimentation. In the first phase density profiles (density, ρ vs. depth, z) were measured to determine the depth of formation and rate of lowering of the density jump, or "interface" between the homogeneous upper layer and the stably stratified bottom layer, and are necessary for the determination of the Richardson number. In the second phase velocity profiles (mean velocity, $\overline{U}$ vs. depth, z) were measured for both the stratified and unstratified situations to show the differences in flow distribution. At the same time turbulent fluctuations u' were recorded to determine the horizontal turbulent energy distribution (u'^2 vs. depth, z).

Nine separate data taking runs were performed in the first phase, three runs of different wind duration for each of three different wind velocities. Density profiles were measured simultaneously at three locations along the tank, 8 meters, 15 meters, and 22.5 meters from the upwind end of the tank, designated stations 6, 12, and 18,respectively. The profiles show the position of the interface and comparison of two profiles under wind of the same velocity but different durations give the entrainment velocity. Figures 7 through 31 display the density profiles;each Figure shows the profile of the starting conditions, a "steady state" profile at a designated time after the wind was started, and a final profile taken after the wind was stopped and internal oscillations had ceased. Comparison of the corresponding profiles at the three positions along the tank gives the horizontal density structure of the internal setup, illus-

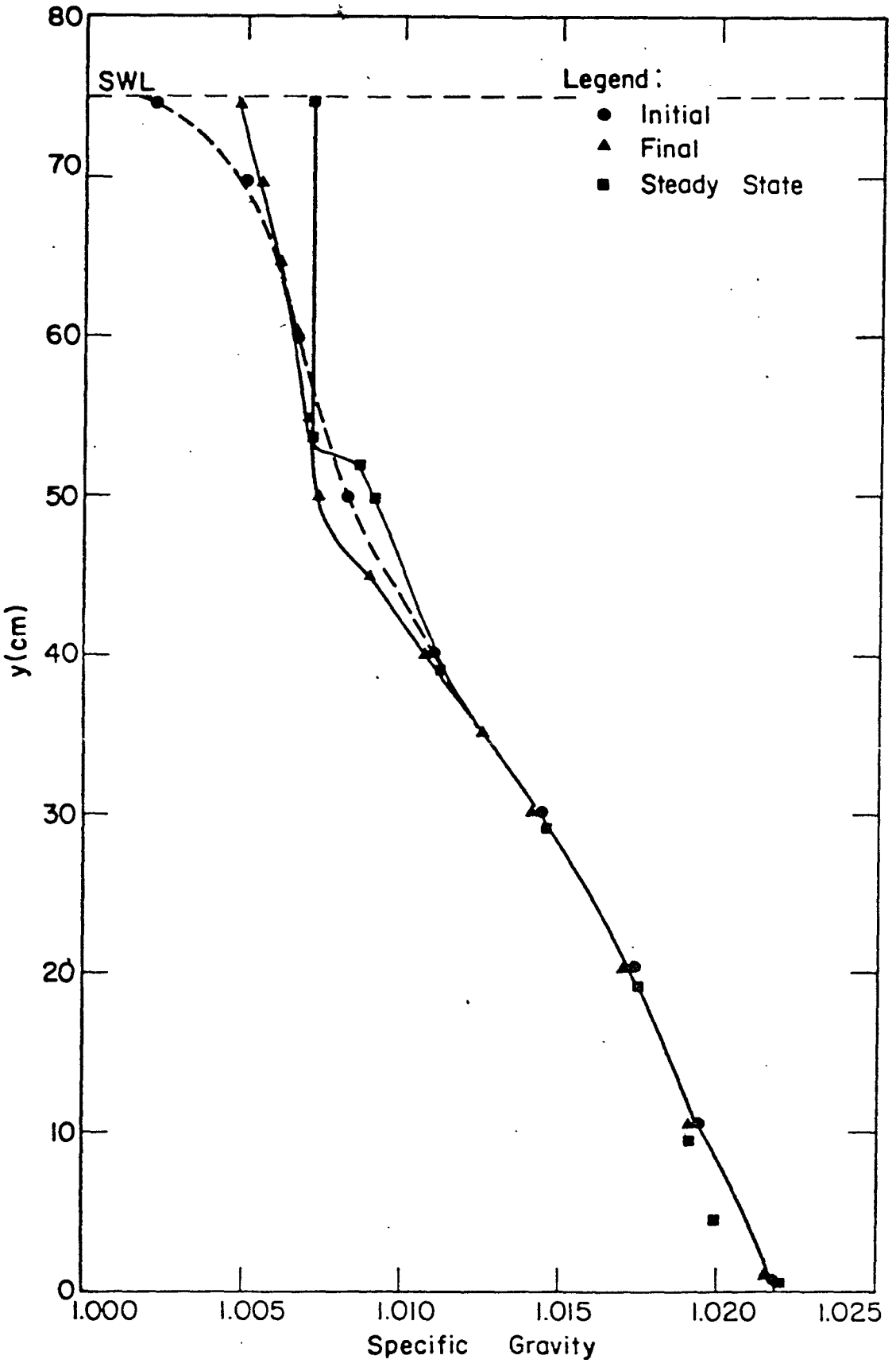

Figure 7. Density profile at Station 6 for wind duration 3 hours, wind velocity 2 mps.

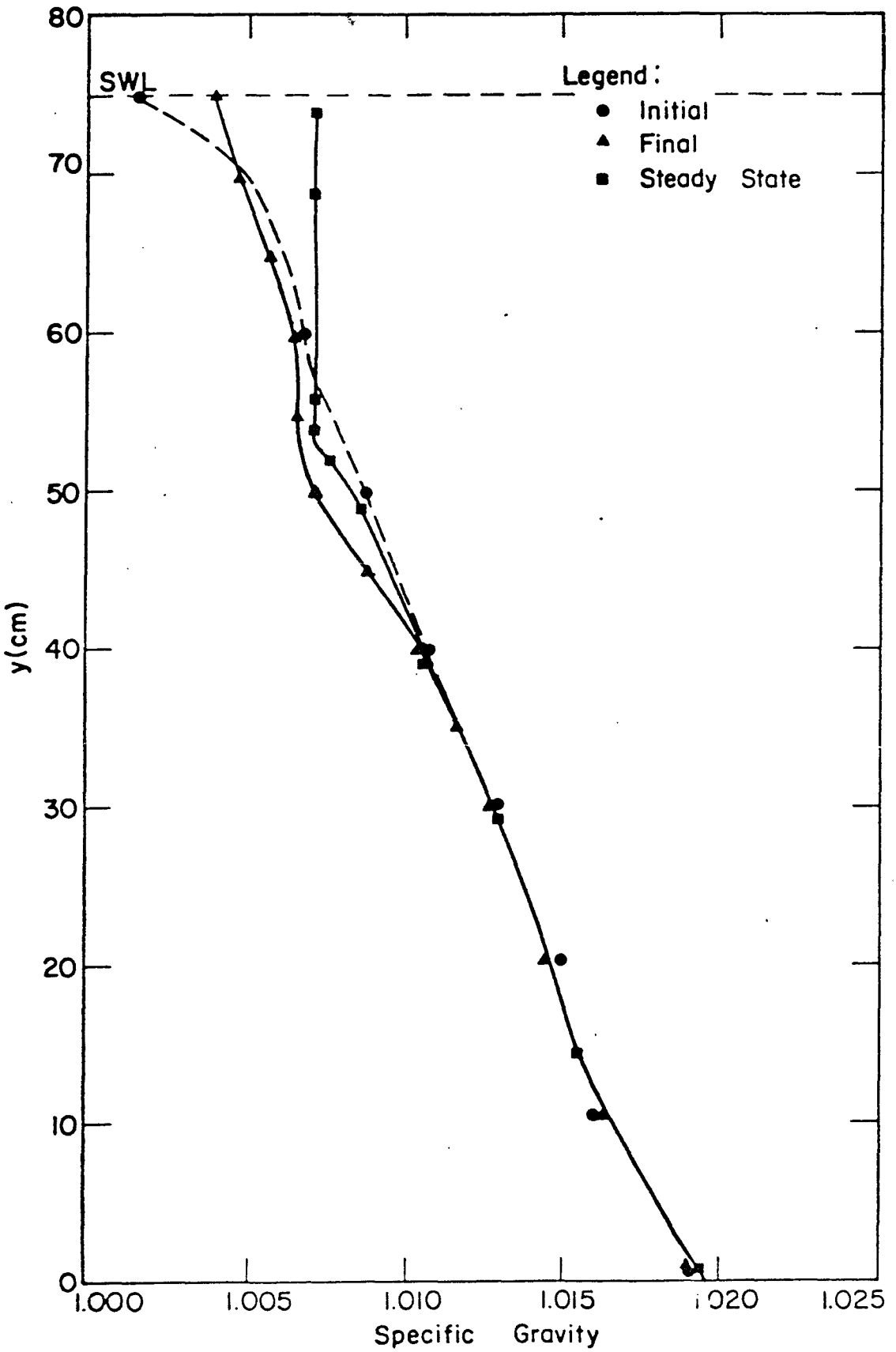

Figure 8. Density profile at Station 6 for wind duration 4 hours, wind velocity 2 mps.

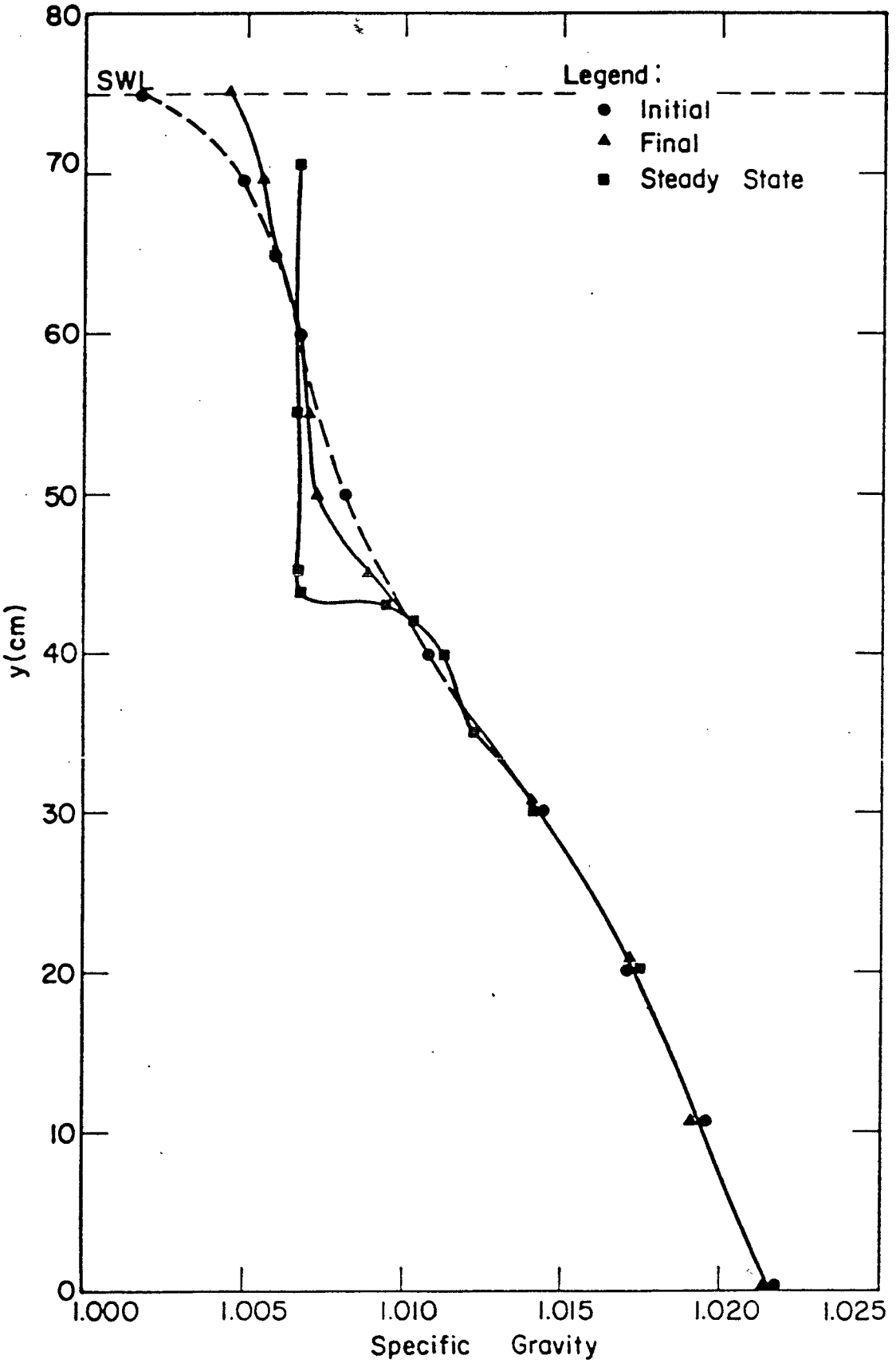

Figure 9. Density profile at Station 12 for wind duration 3 hours, wind velocity 2 mps.

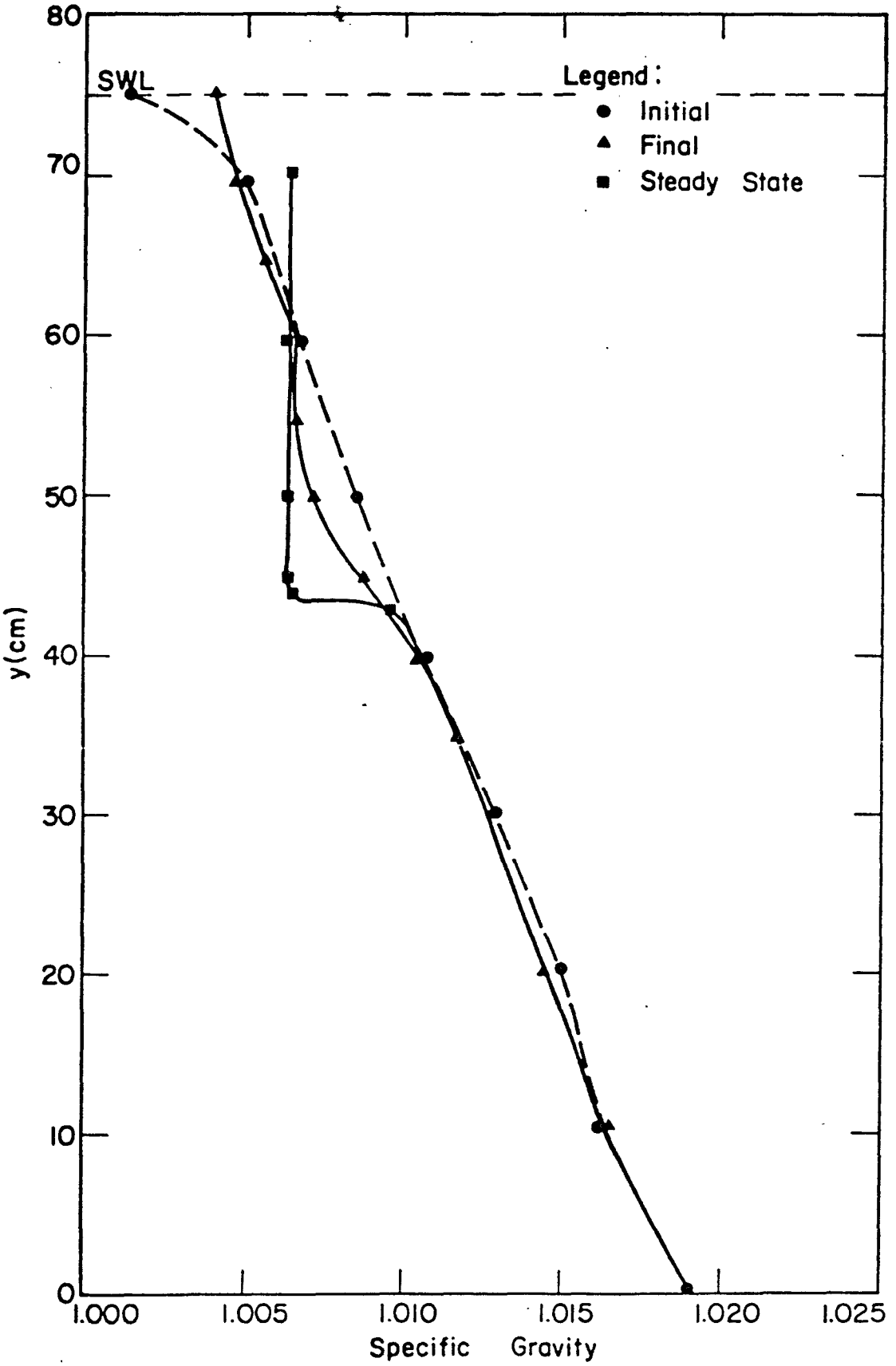

Figure 10. Density profile at Station 12 for wind duration 4 hours, wind velocity 2 mps.

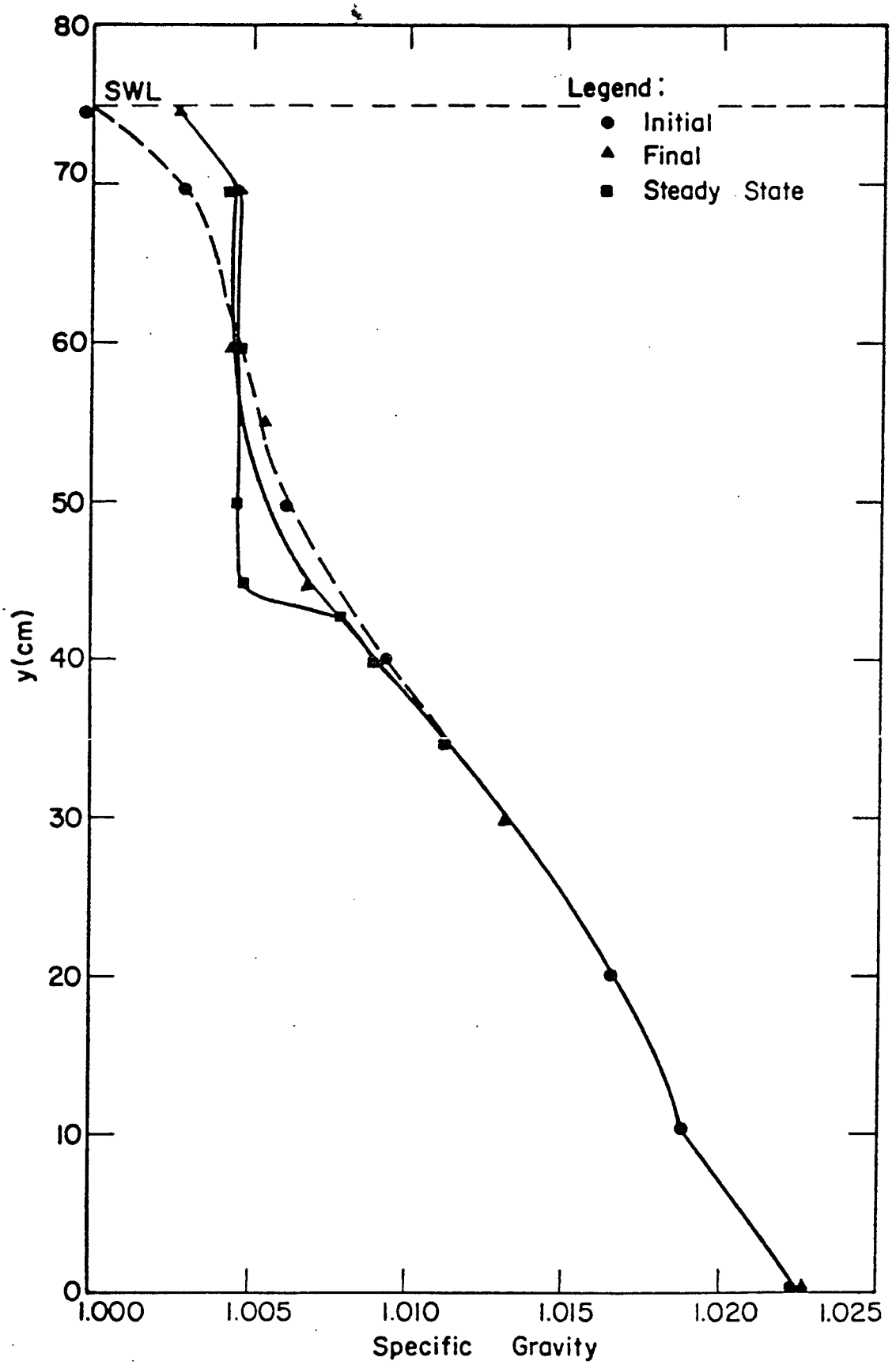

Figure 11. Density profile at Station 12 for wind duration 5 hours, wind velocity 2 mps.

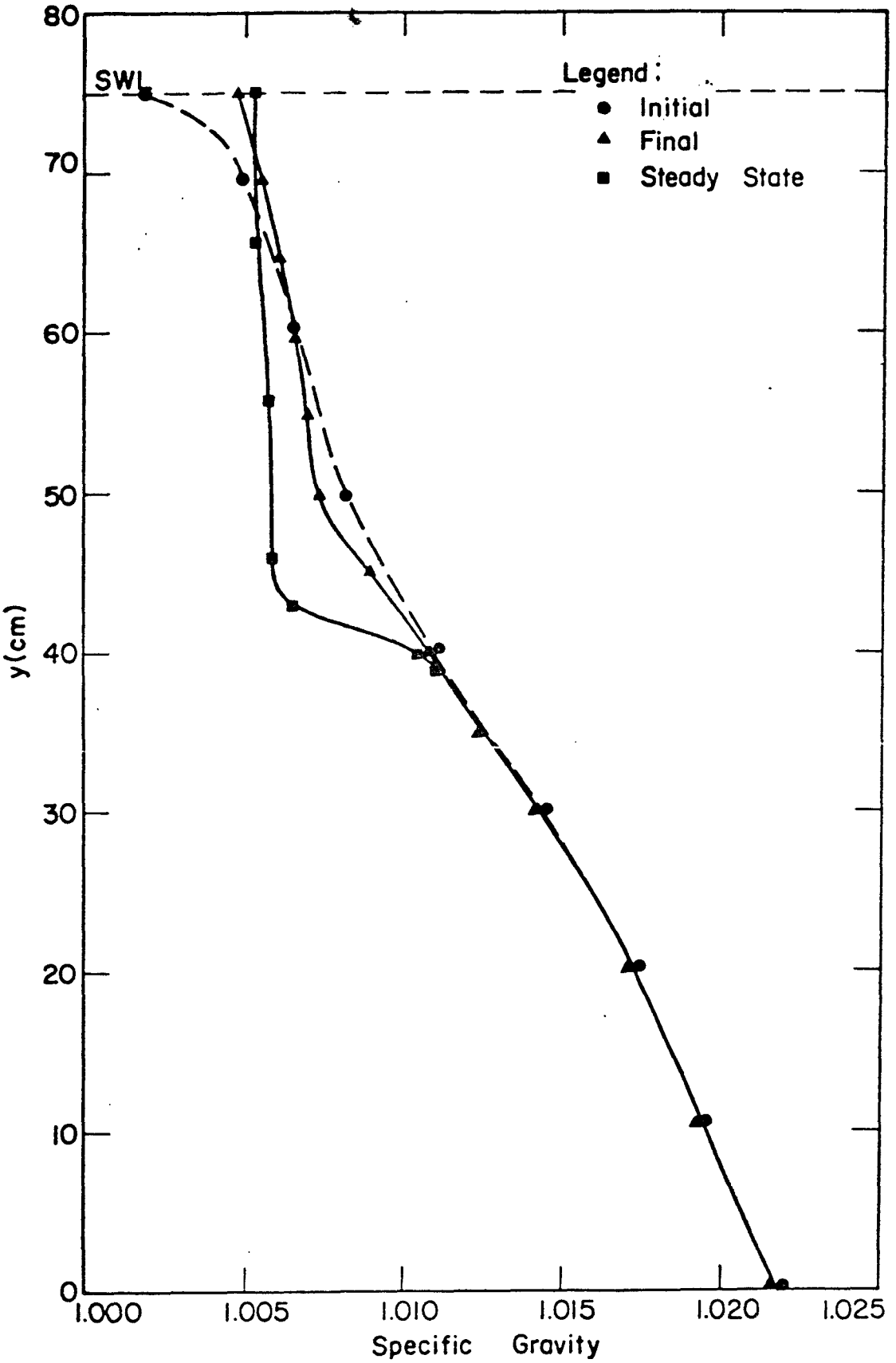

Figure 12. Density Profile at Station 18 for wind duration 3 hours, wind velocity 2 mps.

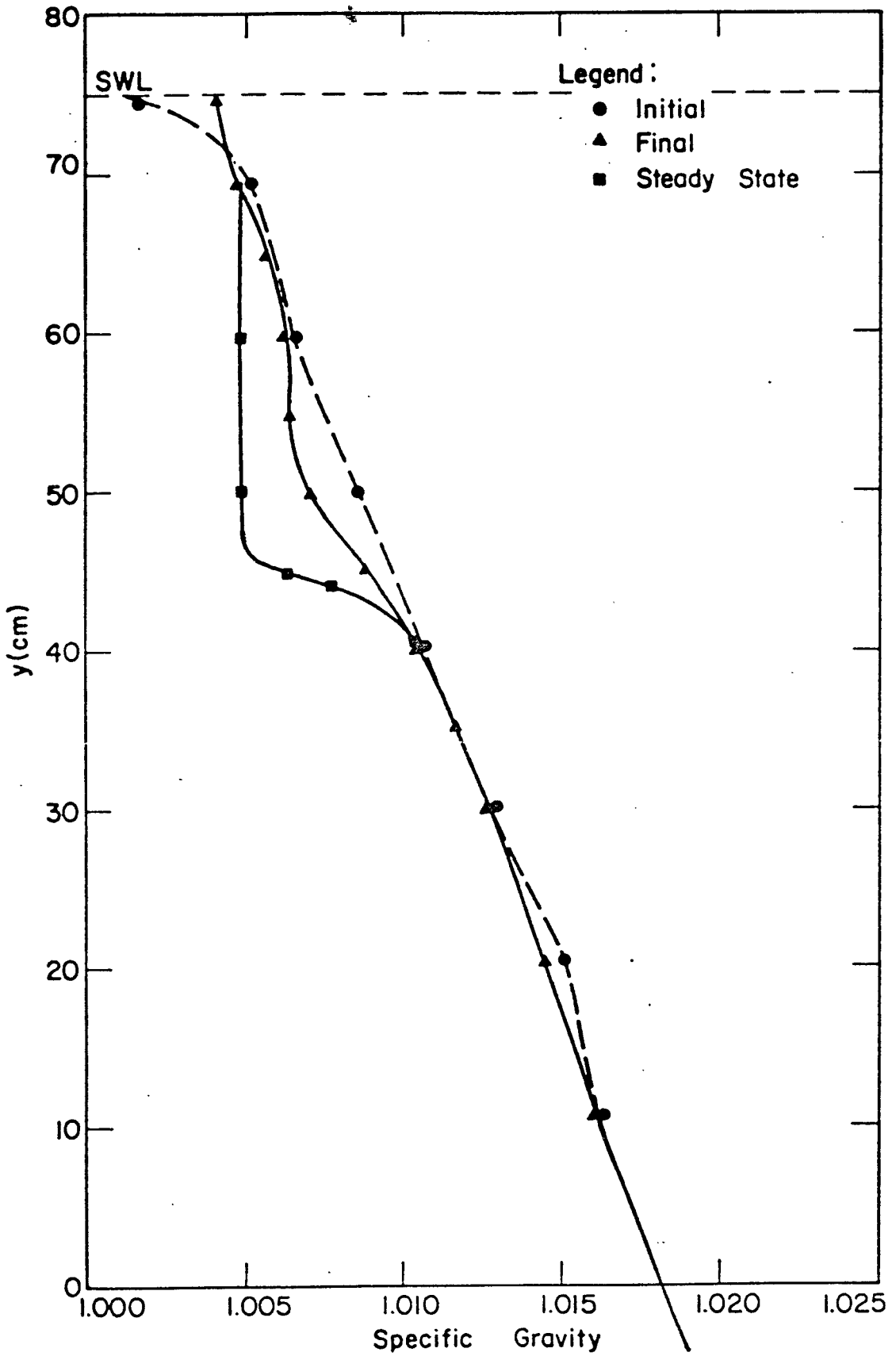

Figure 13. Density profile at Station 18 for wind duration 4 hours, wind velocity 2 mps.

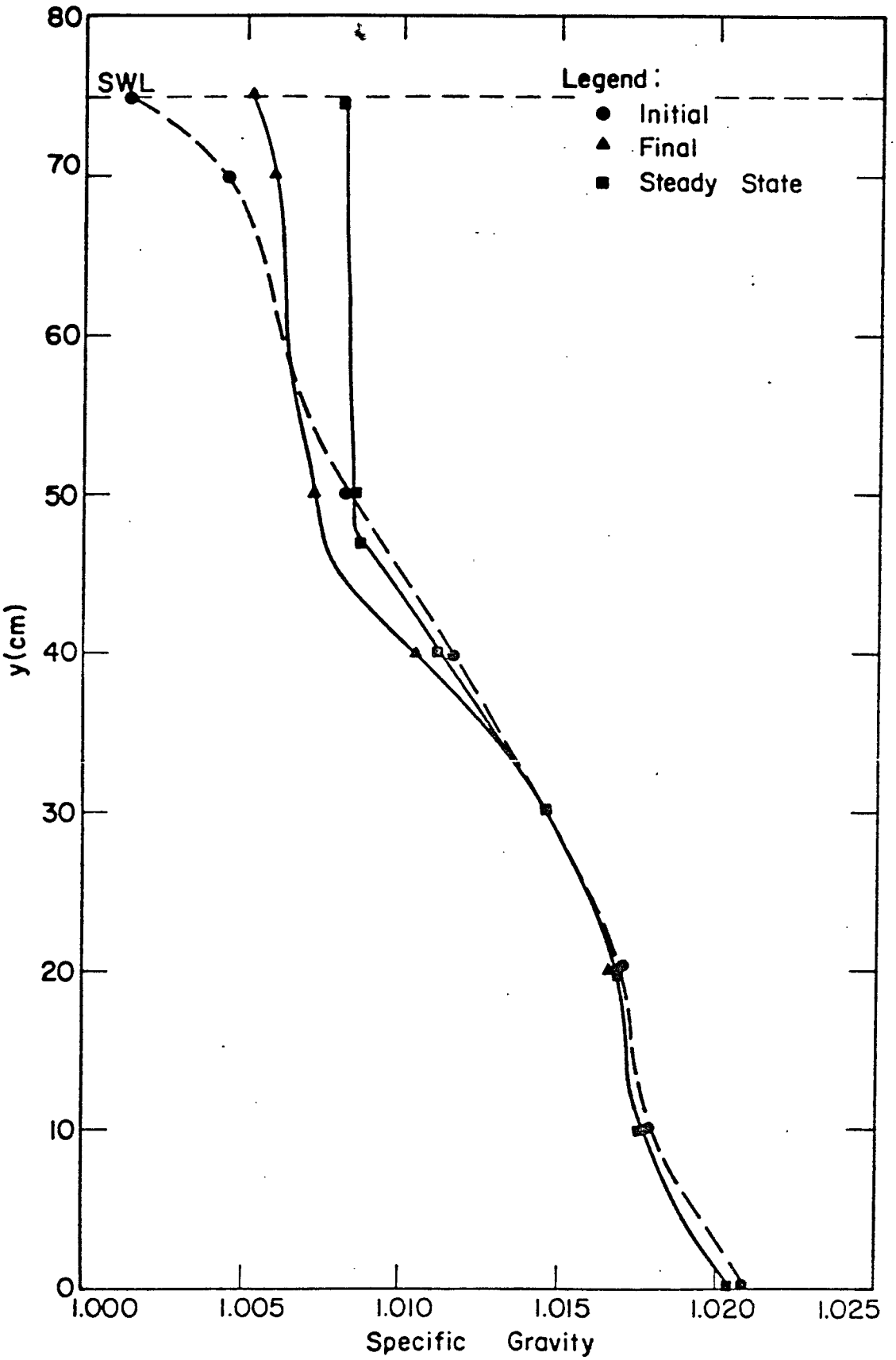

Figure 14. Density profile at Station 6 for wind duration 3 hours, wind velocity 2.5 mps.

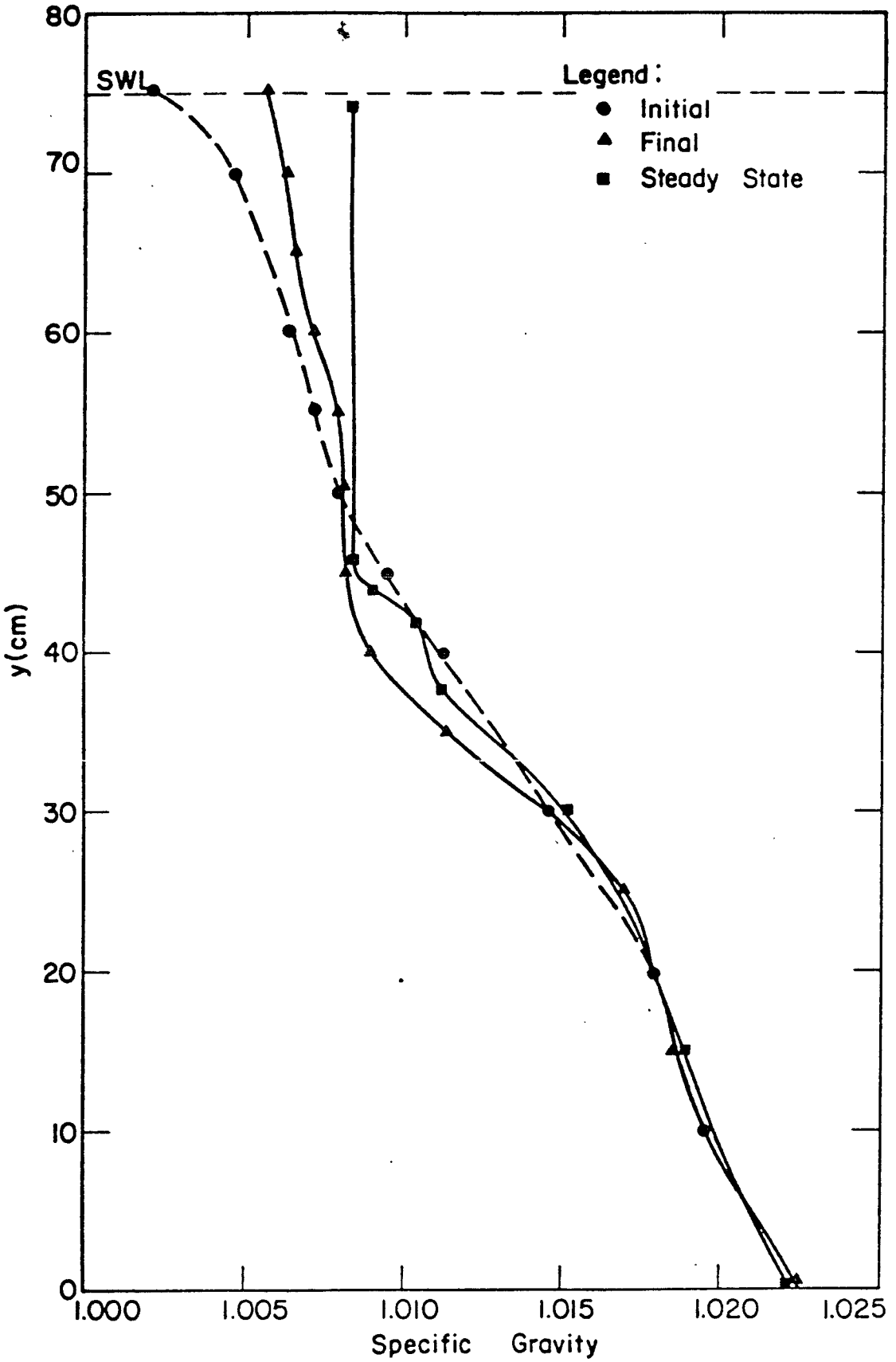

Figure 15. Density profile at Station 6 for wind duration 4 hours, wind velocity 2.5 mps.

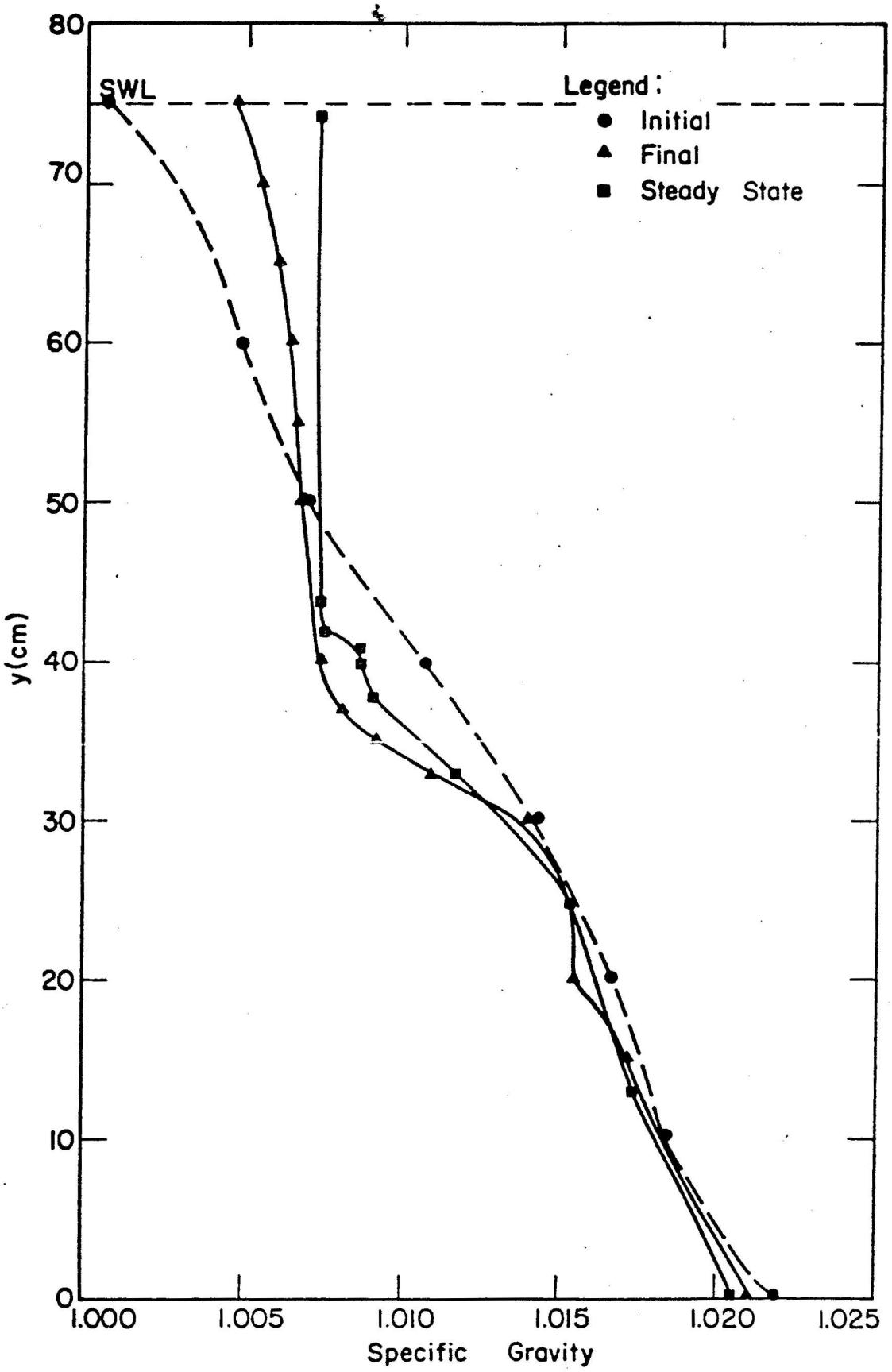

Figure 16. Density profile at Station 6 for wind duration 5 hours, wind velocity 2.5 mps.

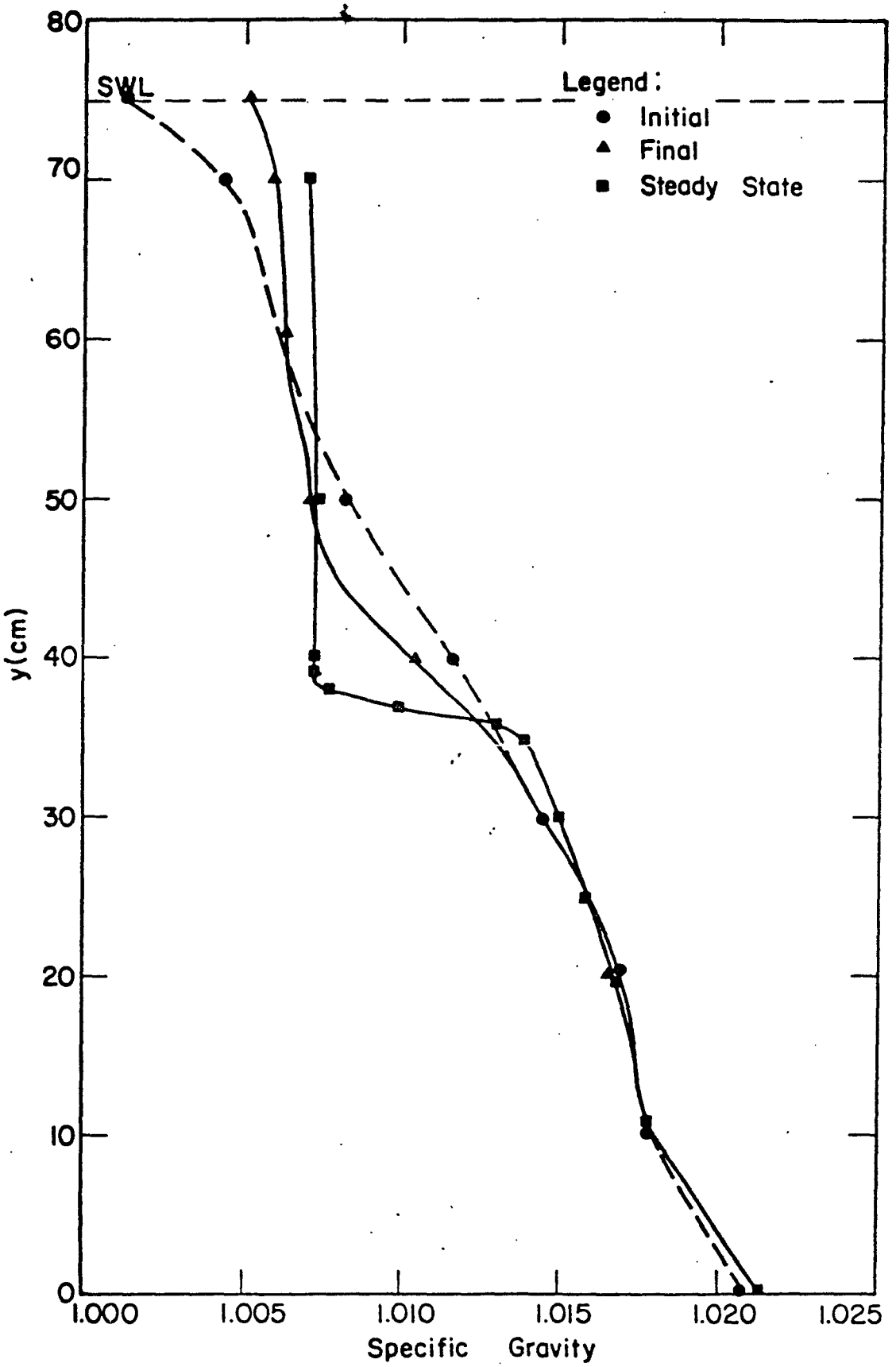

Figure 17. Density profile at Station 12 for wind duration 3 hours, wind velocity 2.5 mps.

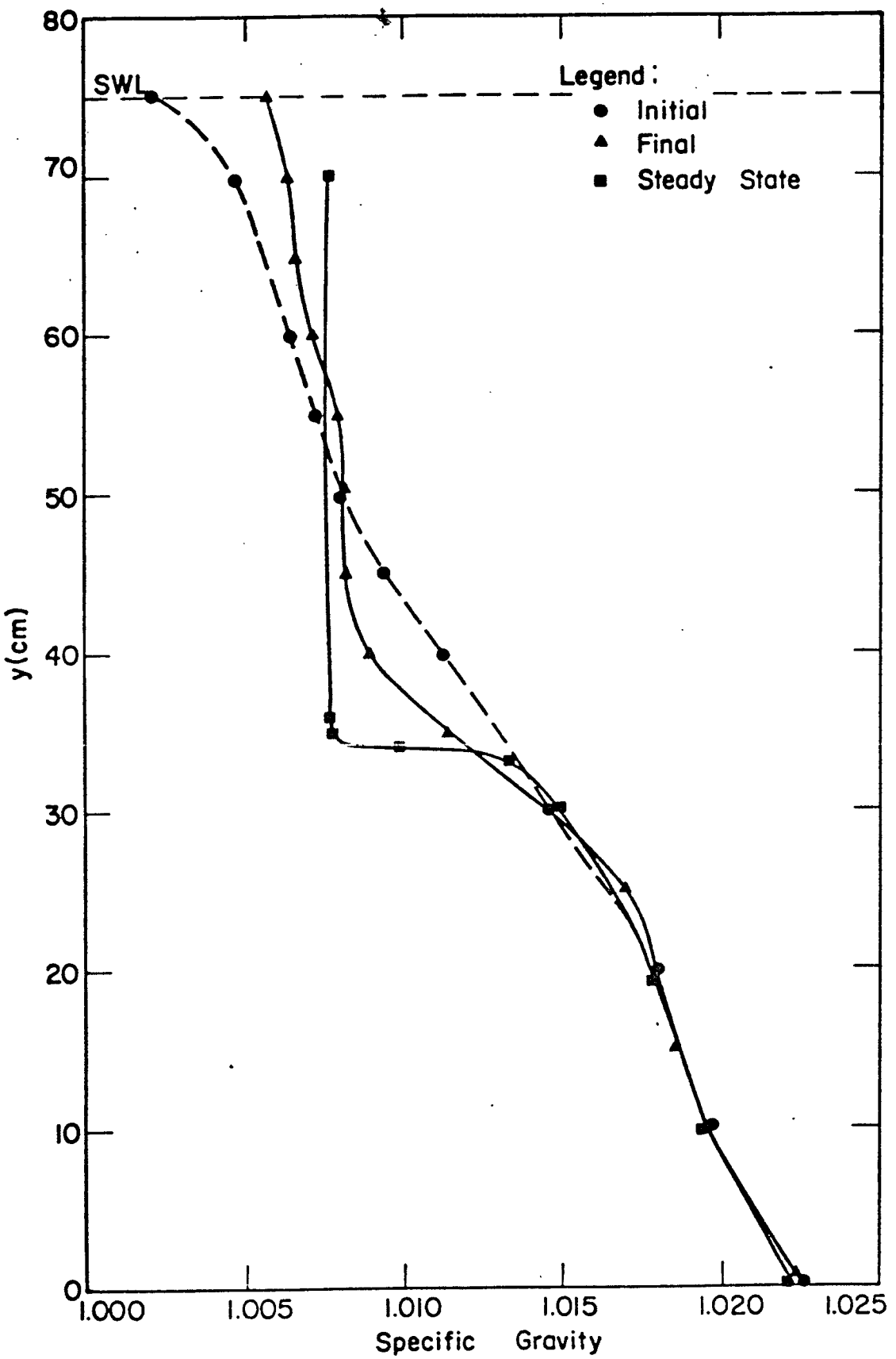

Figure 18. Density profile at Station 12 for wind duration 4 hours, wind velocity 2.5 mps.

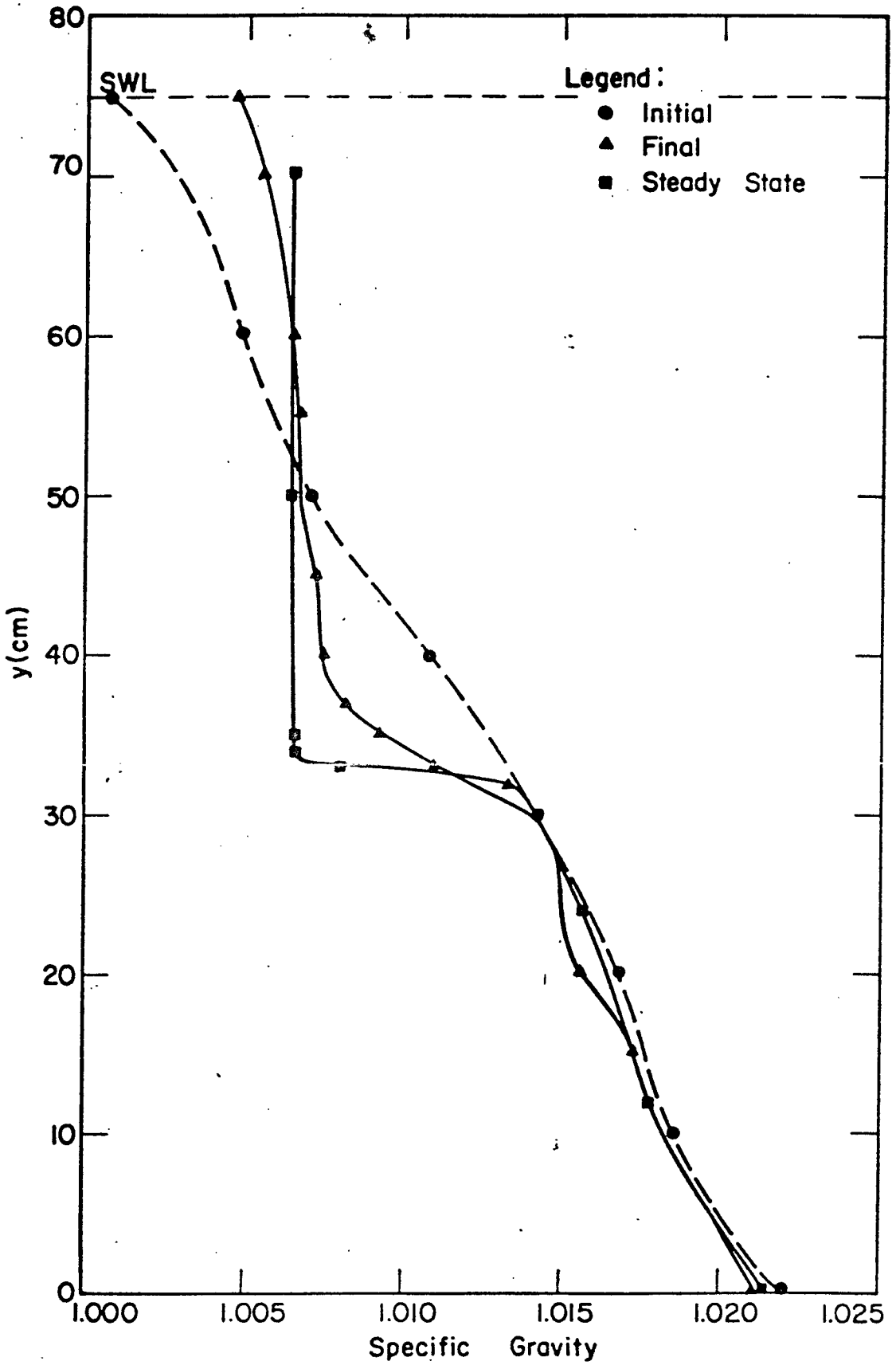

Figure 19. Density profile at Station 12 for wind duration 5 hours, wind velocity 2.5 mps.

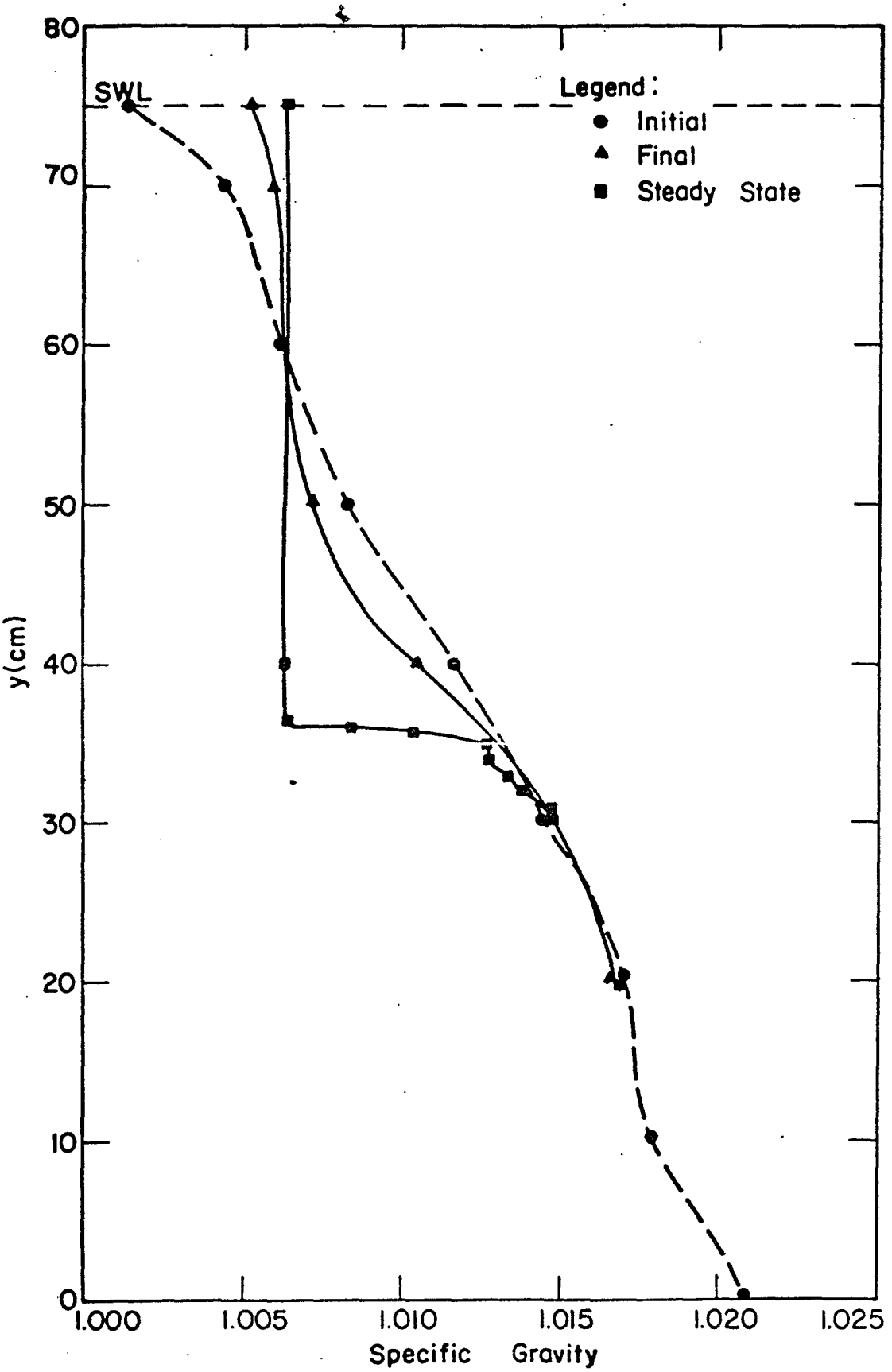

Figure 20. Density profile at Station 18 for wind duration 3 hours, wind velocity 2.5 mps.

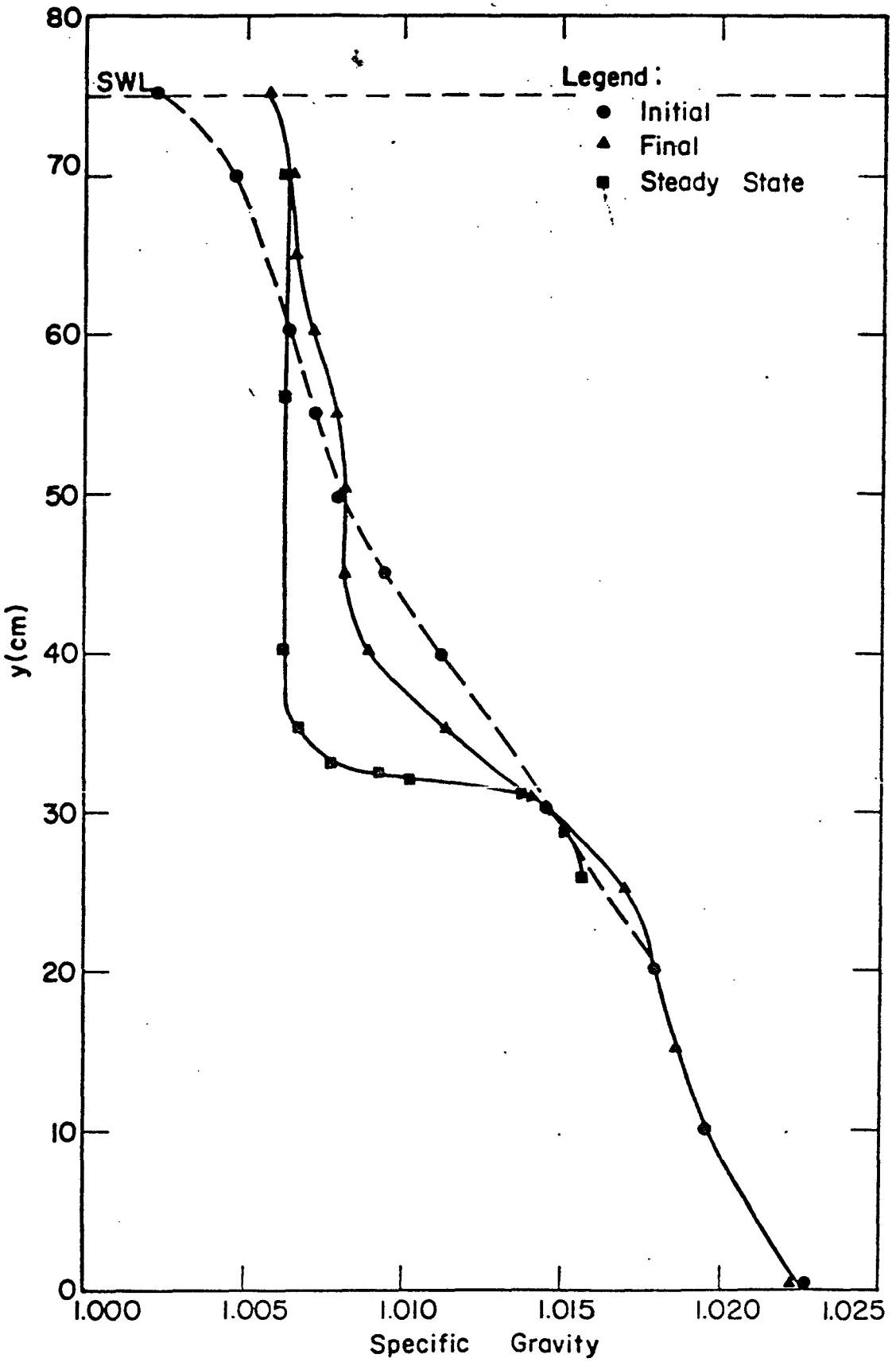

Figure 21. Density profile at Station 18 for wind duration 4 hours, wind velocity 2.5 mps..

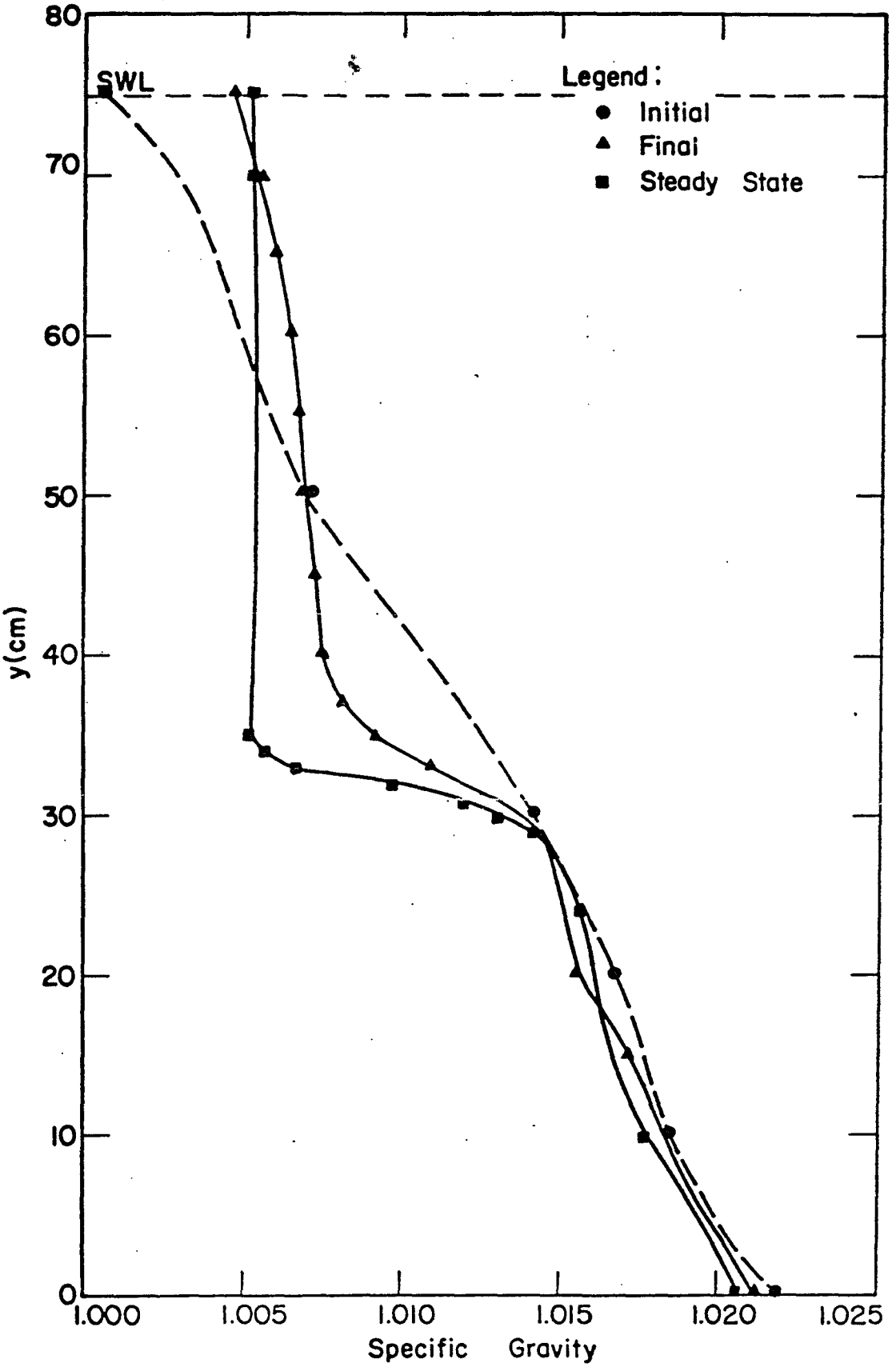

Figure 22. Density profile at Station 18 for wind duration 5 hours, wind velocity 2.5 mps.

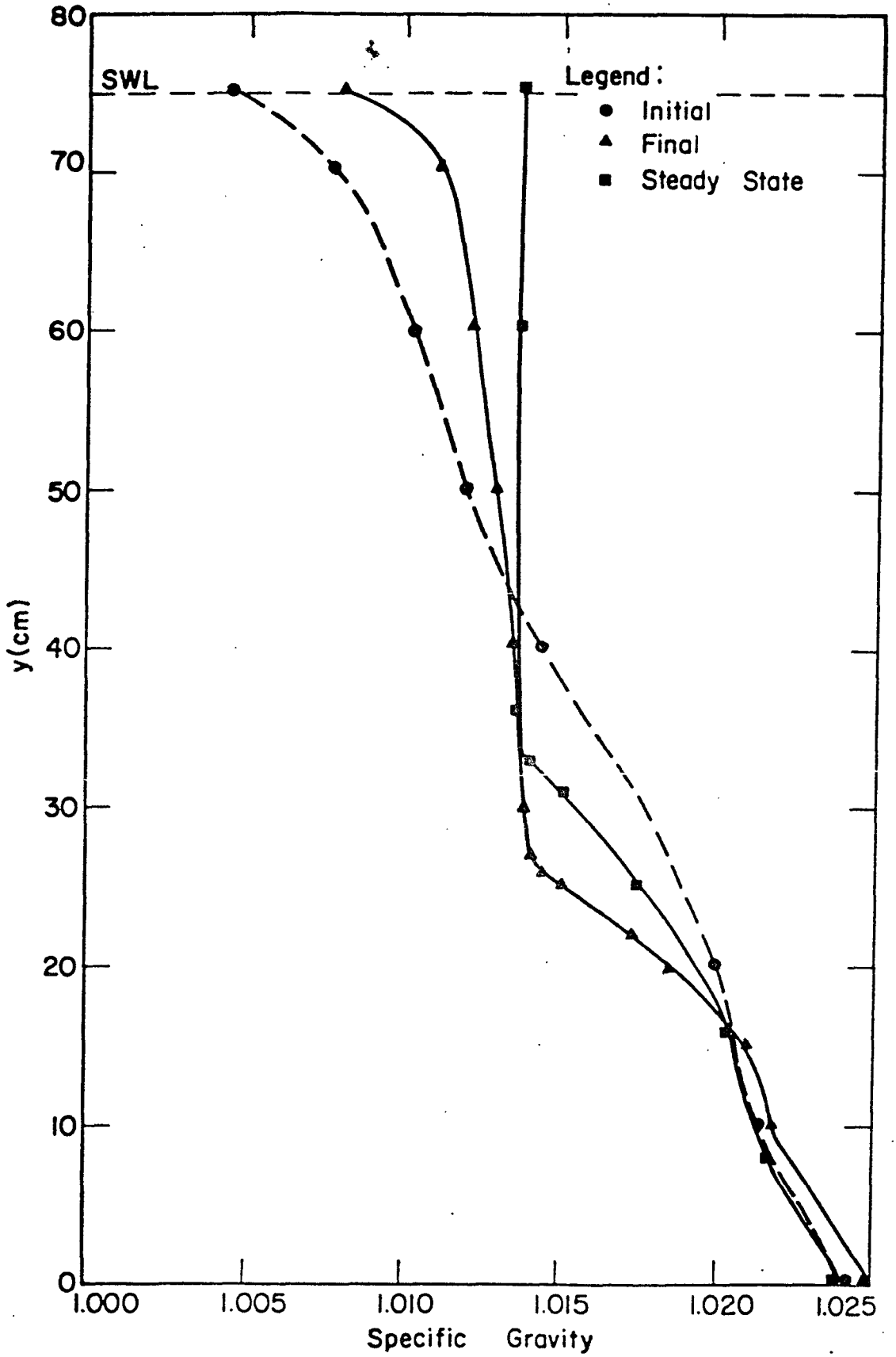

Figure 23. Density profile at Station 6 for wind duration 3 hours, wind velocity 3 mps.

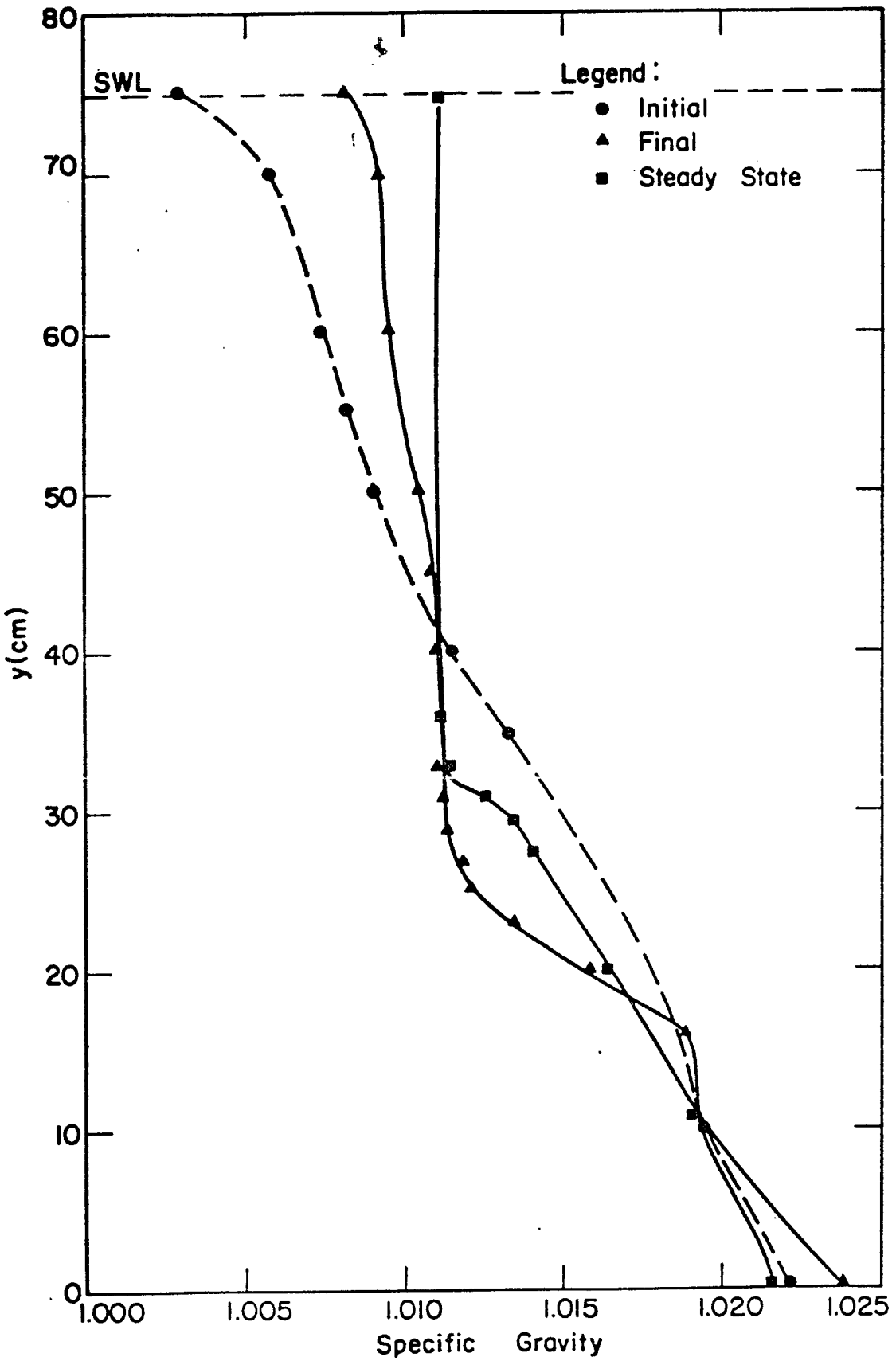

Figure 24. Density profile at Station 6 for wind duration 4 hours, wind velocity 3 mps.

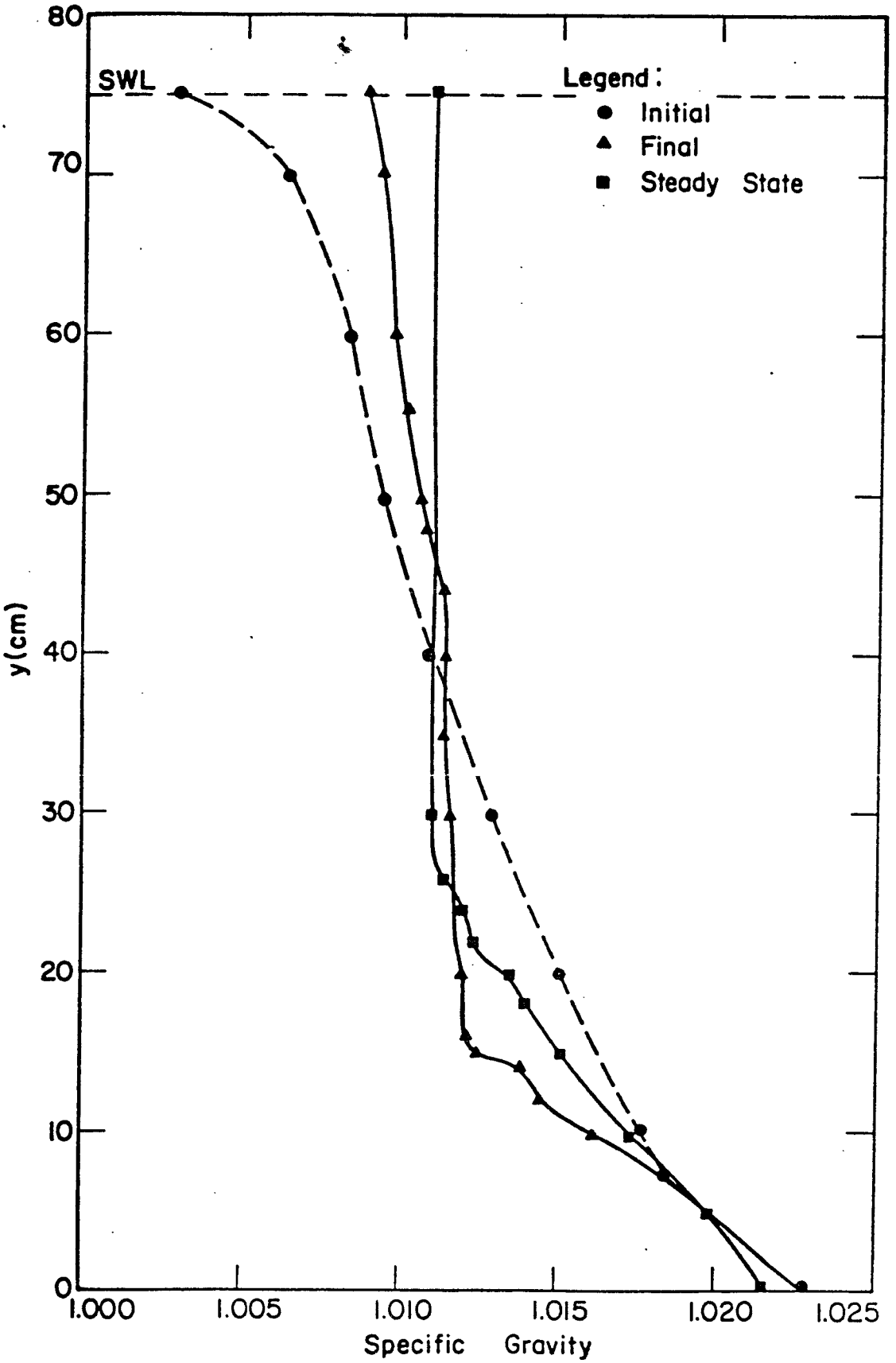

Figure 25. Density profile at Station 6 for wind duration 5 hours, wind velocity 3 mps.

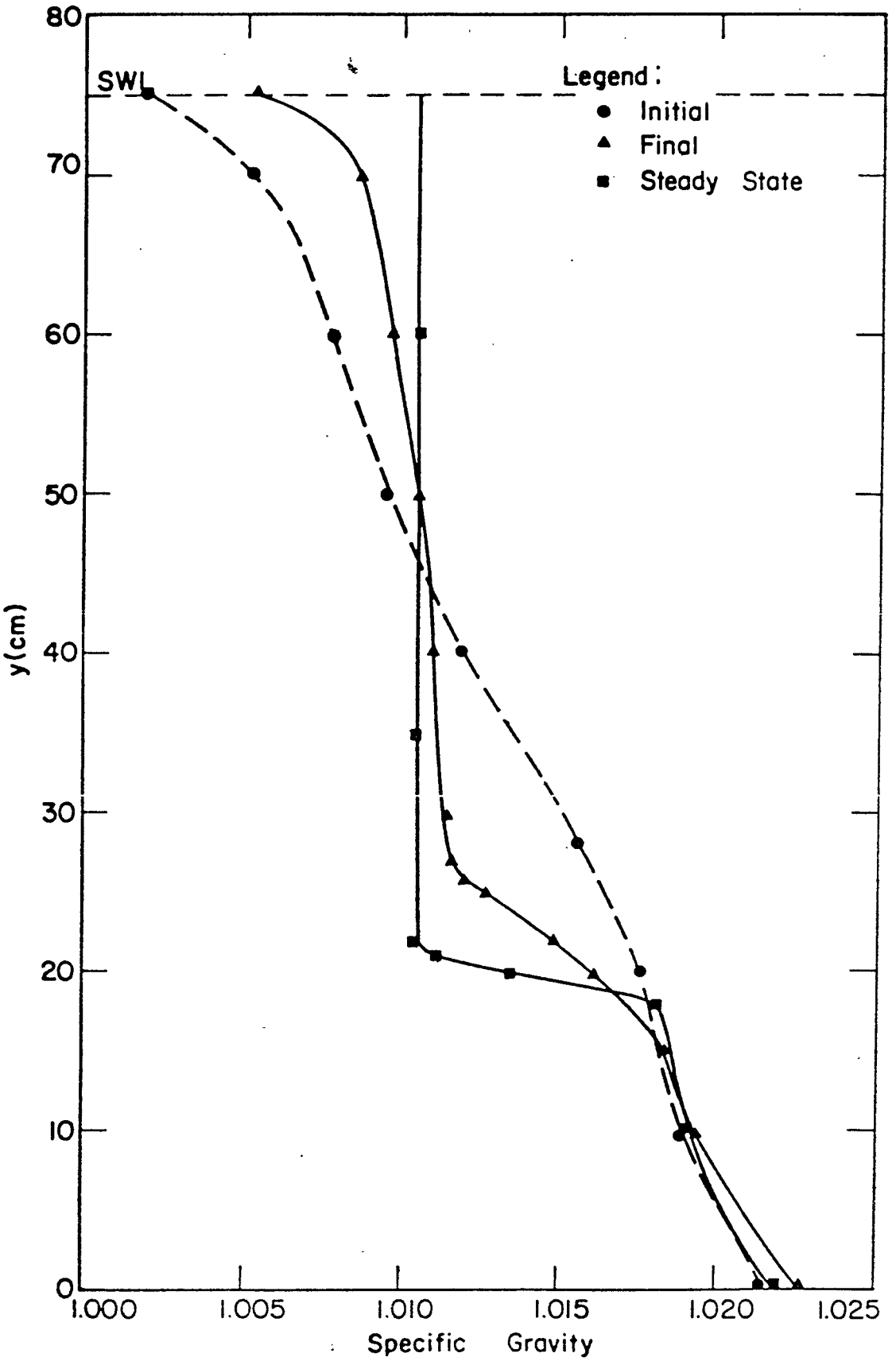

Figure 26. Density profile at Station 12 for wind duration 3 hours, wind velocity 3 mps.

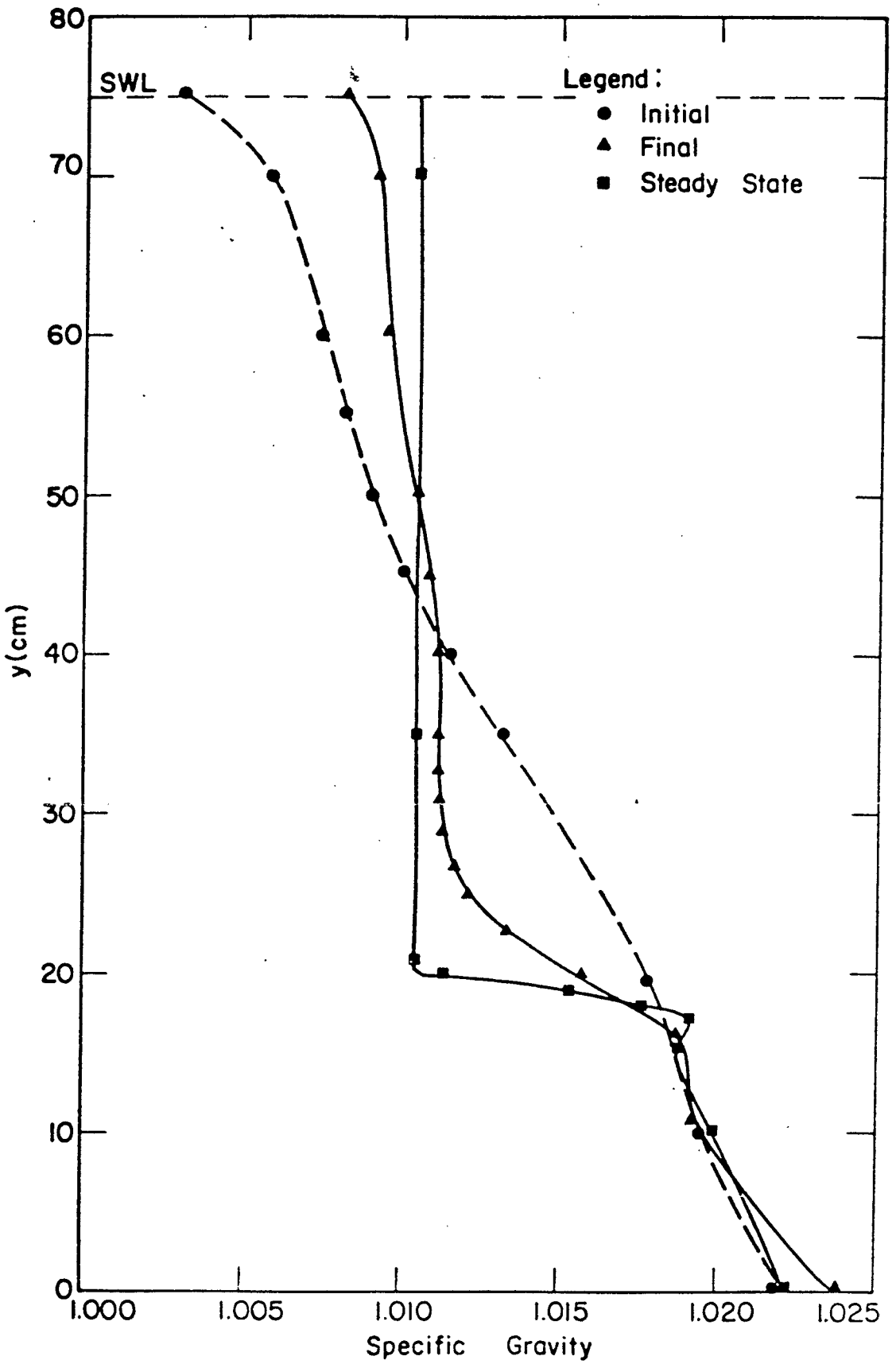

Figure 27. Density profile at Station 12 for wind duration 4 hours, wind velocity 3 mps.

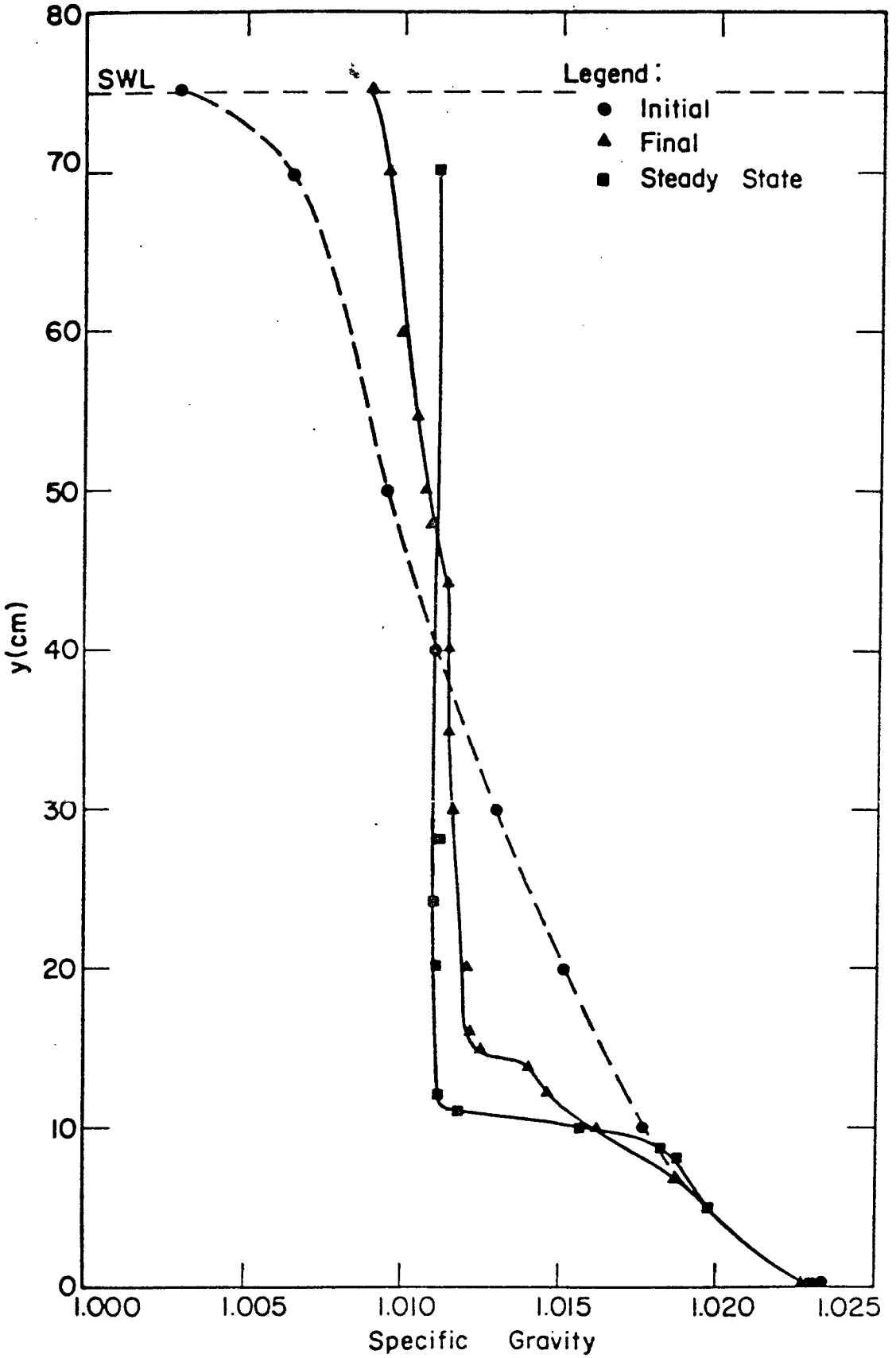

Figure 28. Density profile at Station 12 for wind duration 5 hours, wind velocity 3 mps.

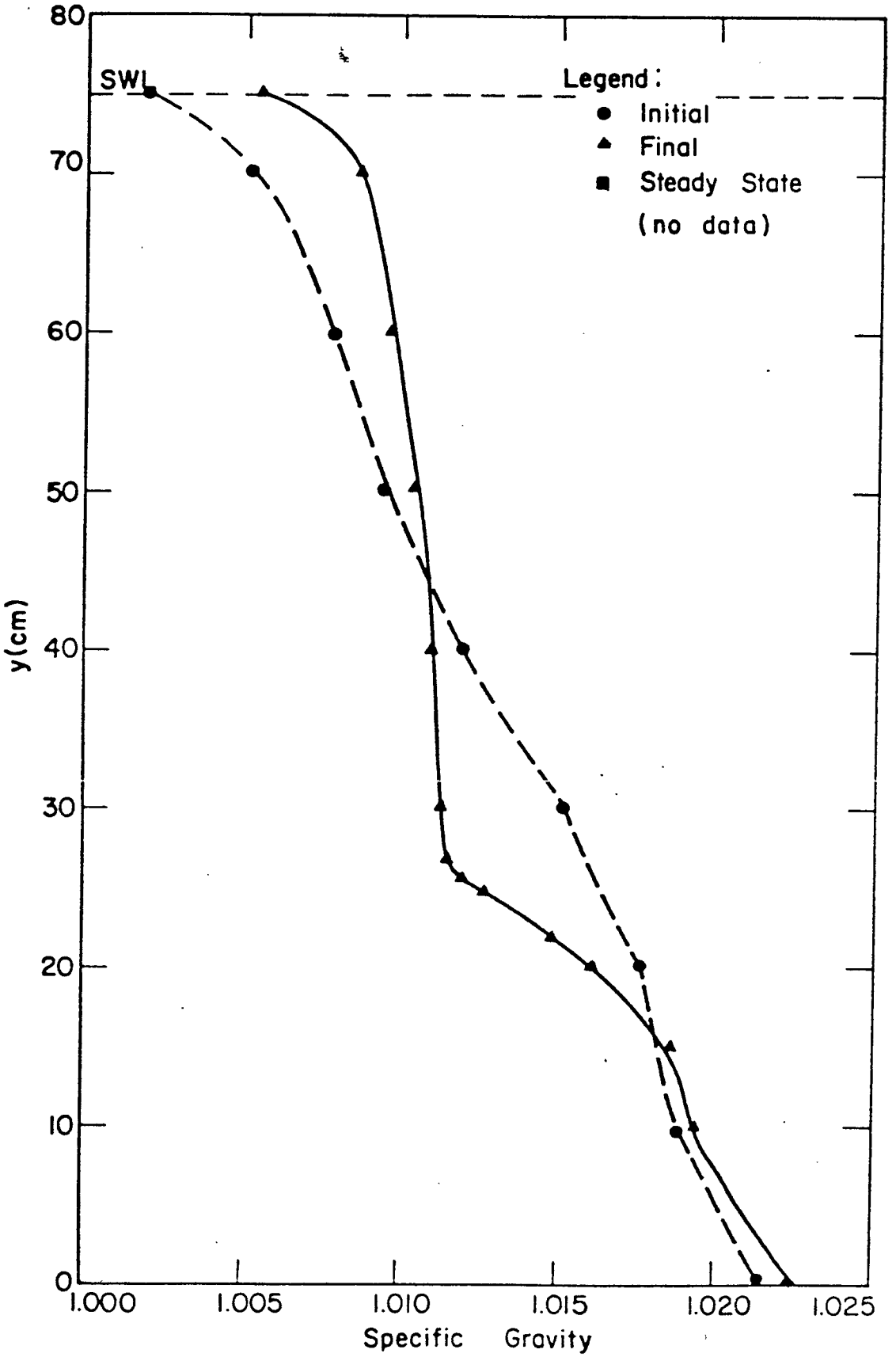

Figure 29. Density profile at Station 18 for wind duration 3 hours, wind velocity 3 mps.

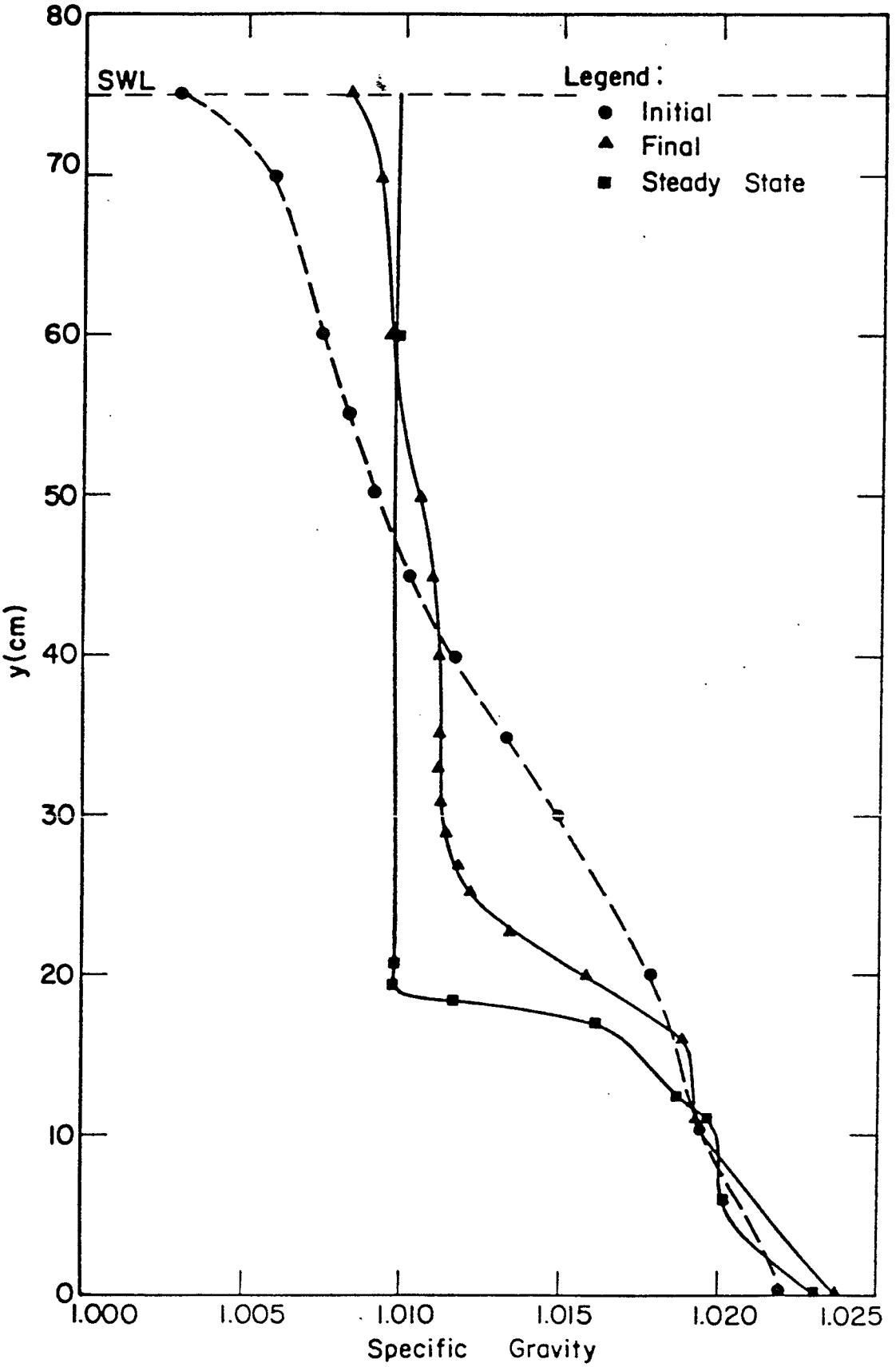

Figure 30. Density profile at Station 18 for wind duration 4 hours, wind velocity 3 mps.

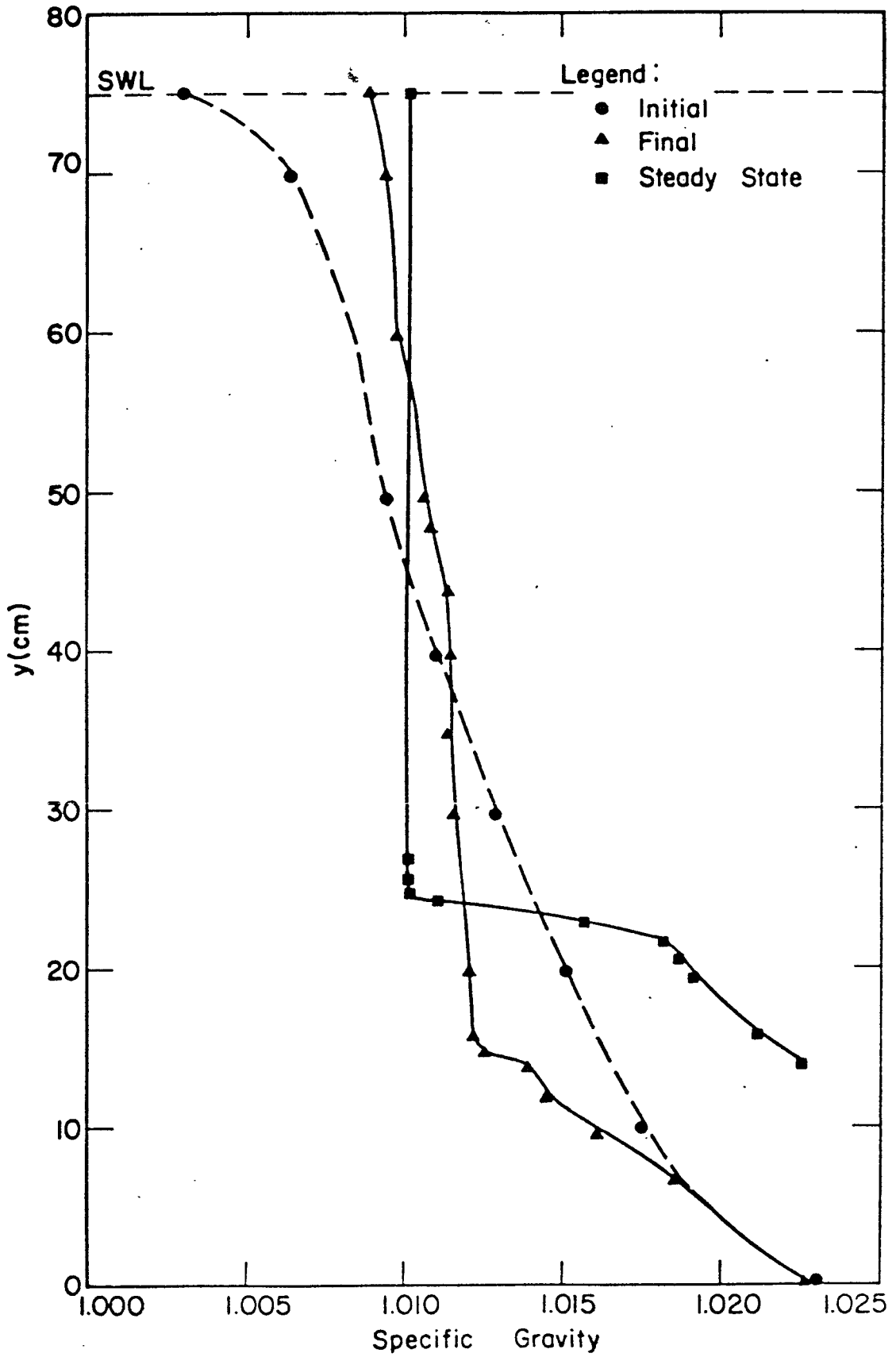

Figure 31. Density profile at Station 18 for wind duration 5 hours, wind velocity 3 mps.

trated for two situations in Figures 32 and 33 as plots of lines of constant density in a two dimensional tank where points with the same density are connected by straight lines for easier identification, although the actual lines of constant density are nonlinear.

The initial density profile for the second phase of experimentation was determined in the same way and is shown in Figure 34, along with a stepwise approximation to the interface for the profiles after the wind had been blowing for 1 and 5 hours. The density of the top layer and the position of the interface were measured; below the interface the density profile was assumed unchanged, which is a reasonable assumption based on the data from the initial experiments.

Figure 35 is the mean velocity profile for the unstratified situation, as well as the stratified case for two different times during the run. This illustrates the change in the flow which takes place as the interface is eroded. Figure 36 is the rms velocity profile, $\{(u'^2)^{\frac{1}{2}}$ vs. z} for the same situations as Figure 35, but does not show much more than a general trend of decreasing magnitude just below the surface.

A logarithmic plot of height above the water surface vs. mean wind velocity is shown in Figure 36. This was used to determine the shear velocity in air u_{*_a} directly, and the shear velocity in water from (Shemdin, 1972)

$$u_{*_w}^2 = \frac{\rho_a}{\rho_w} u_{*_w}^2$$

The turbulent velocity fluctuations u' were analyzed on the spectrum analyzer. The output is plotted in Figures 38 through 41 as the turbulent energy spectra in volt^2-sec vs. frequency. Figures 38, 39, 40 and 41 are the spectra at depths of 2 cm, 10 cm, 15 cm, and 33 cm, respectively. Each figure shows the difference in the horizontal component of the turbulent

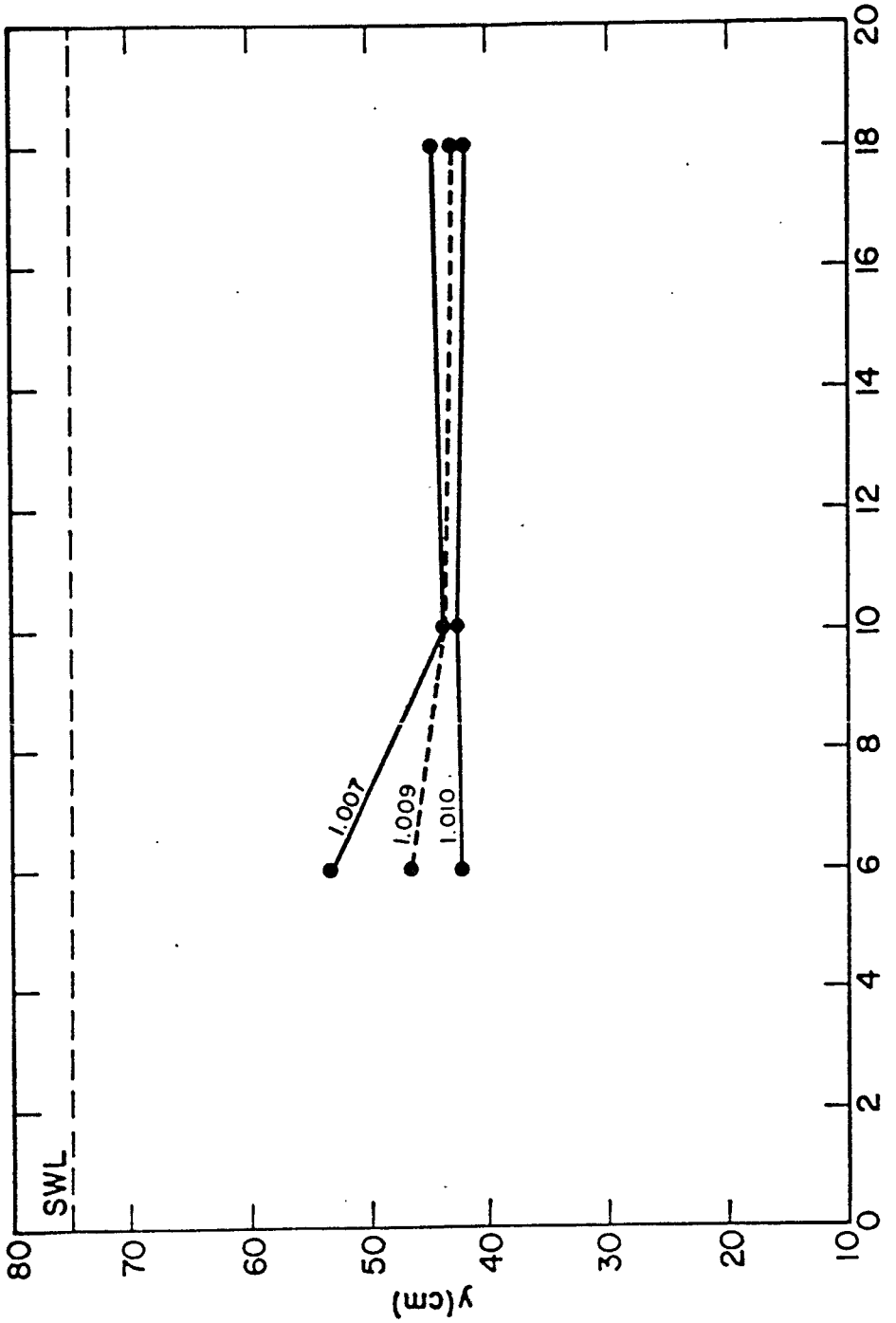

Figure 32. Lines at constant density for wind of 4 hour duration, wind velocity of 2 mps. (See Figures 8, 10, 13.)

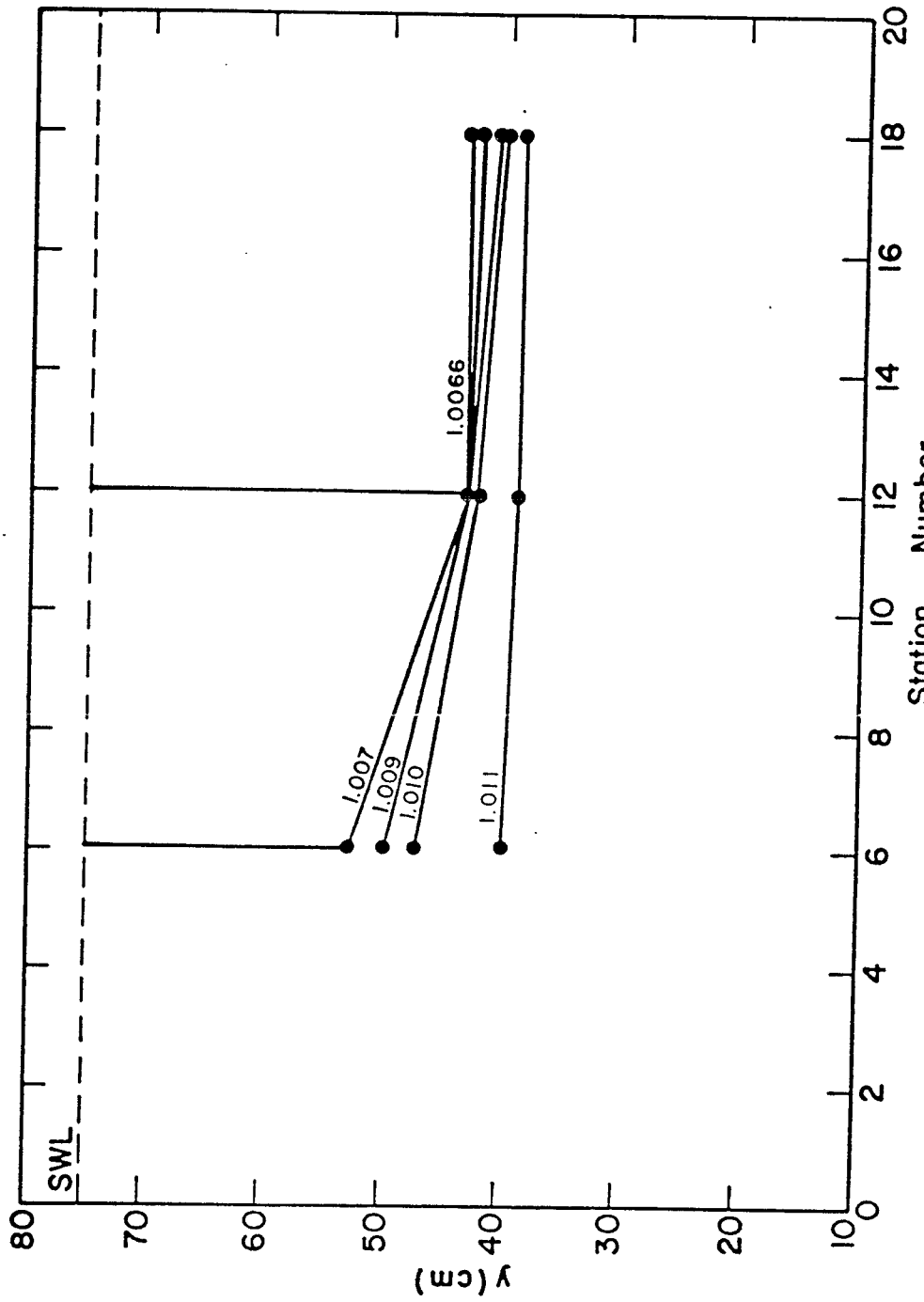

Figure 33. Lines of constant density for wind of 3 hour duration, wind velocity of 2.5 mps. (See Figures 15, 18, 21.)

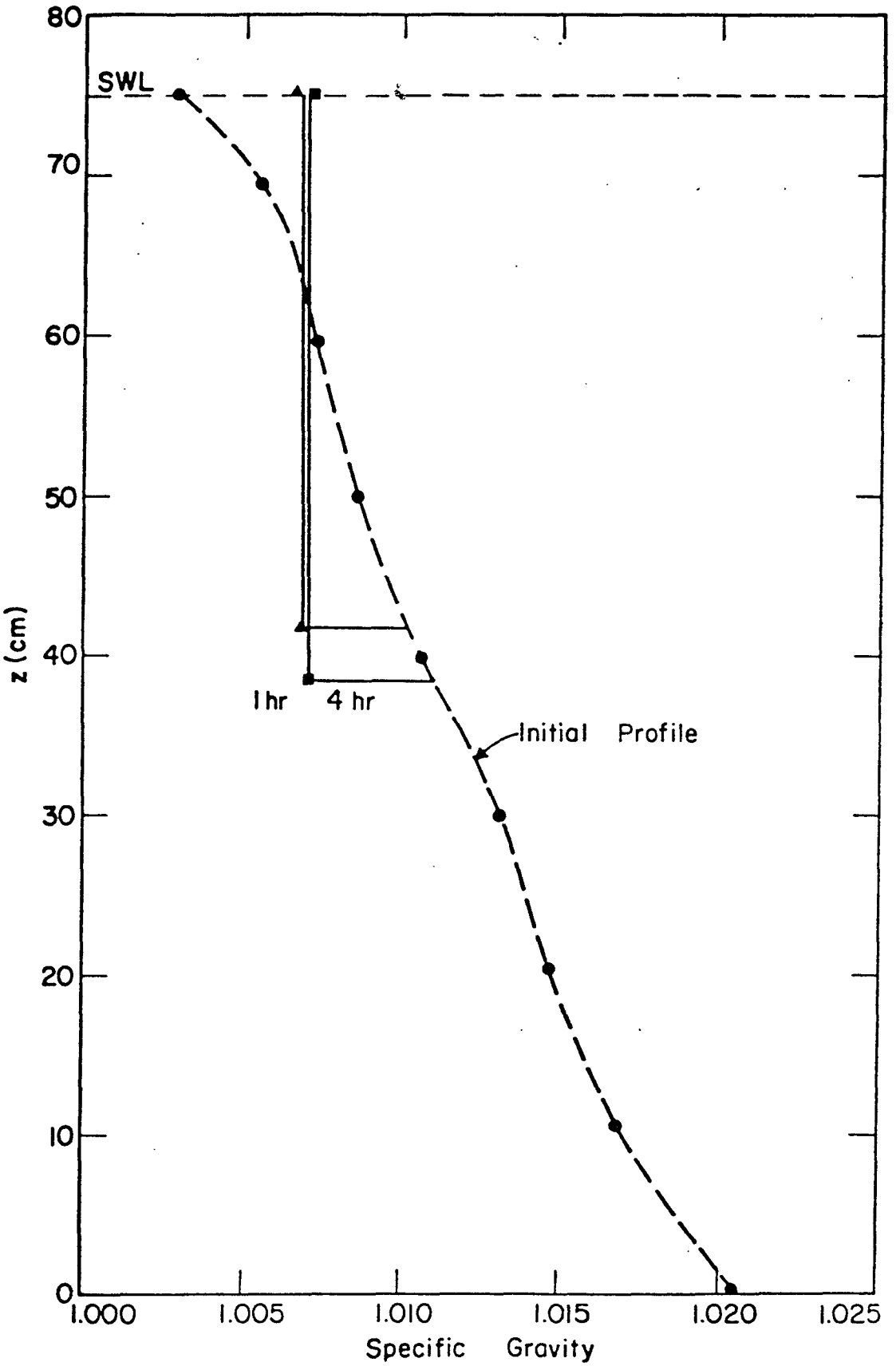

Figure 34. Density profiles for the experimental run during which turbulence measurements were taken.

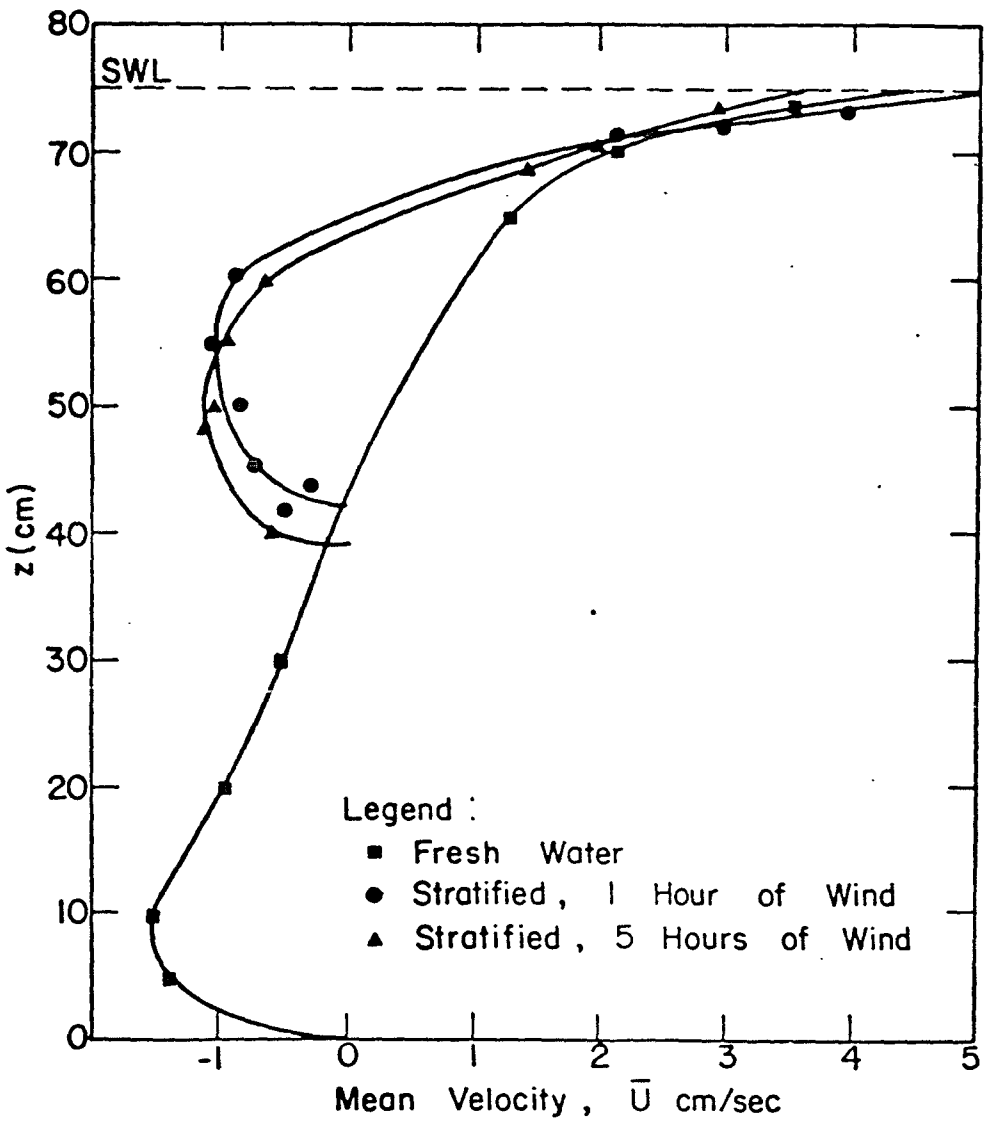

Figure 35. Mean velocity profiles for wind velocity 2.5 mps.

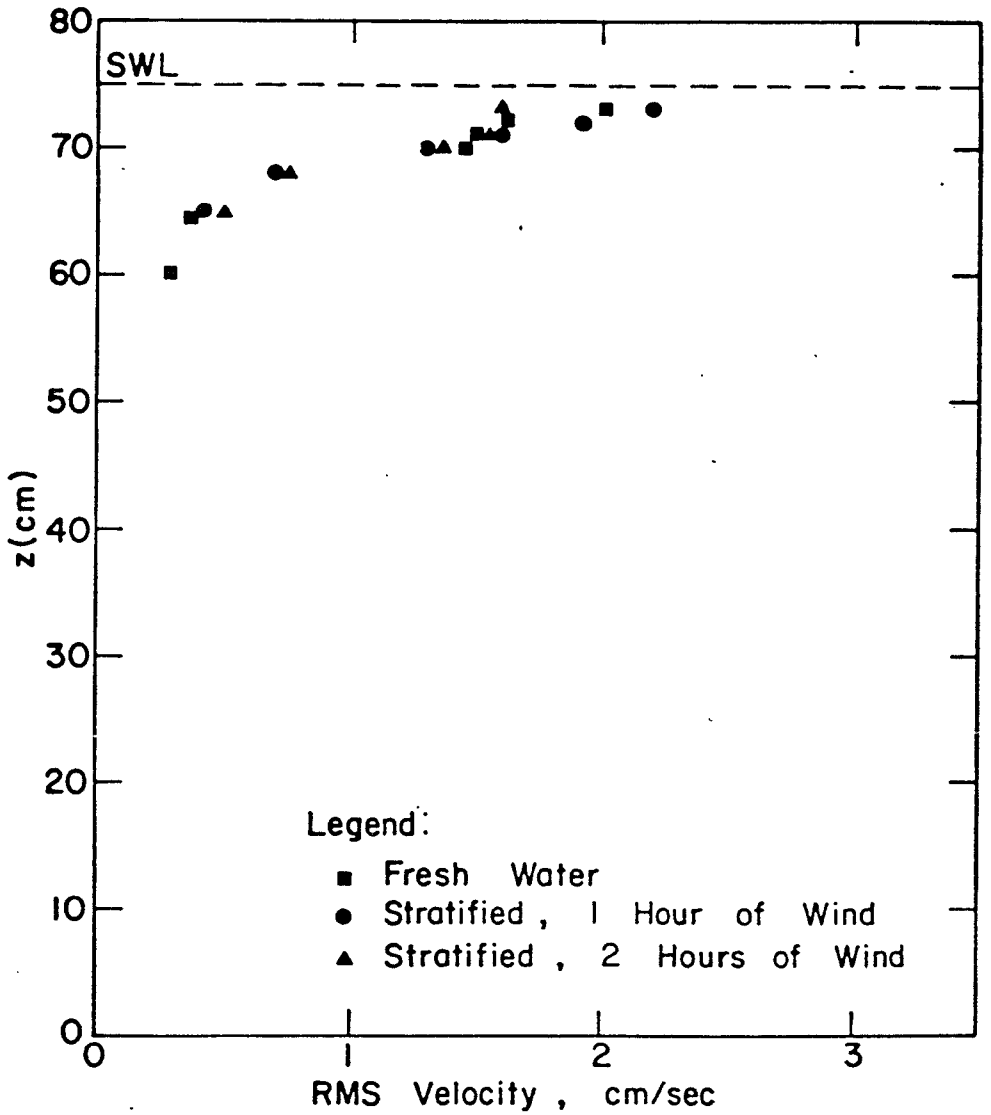

Figure 36. RMS velocities for wind velocity 2.5 mps.

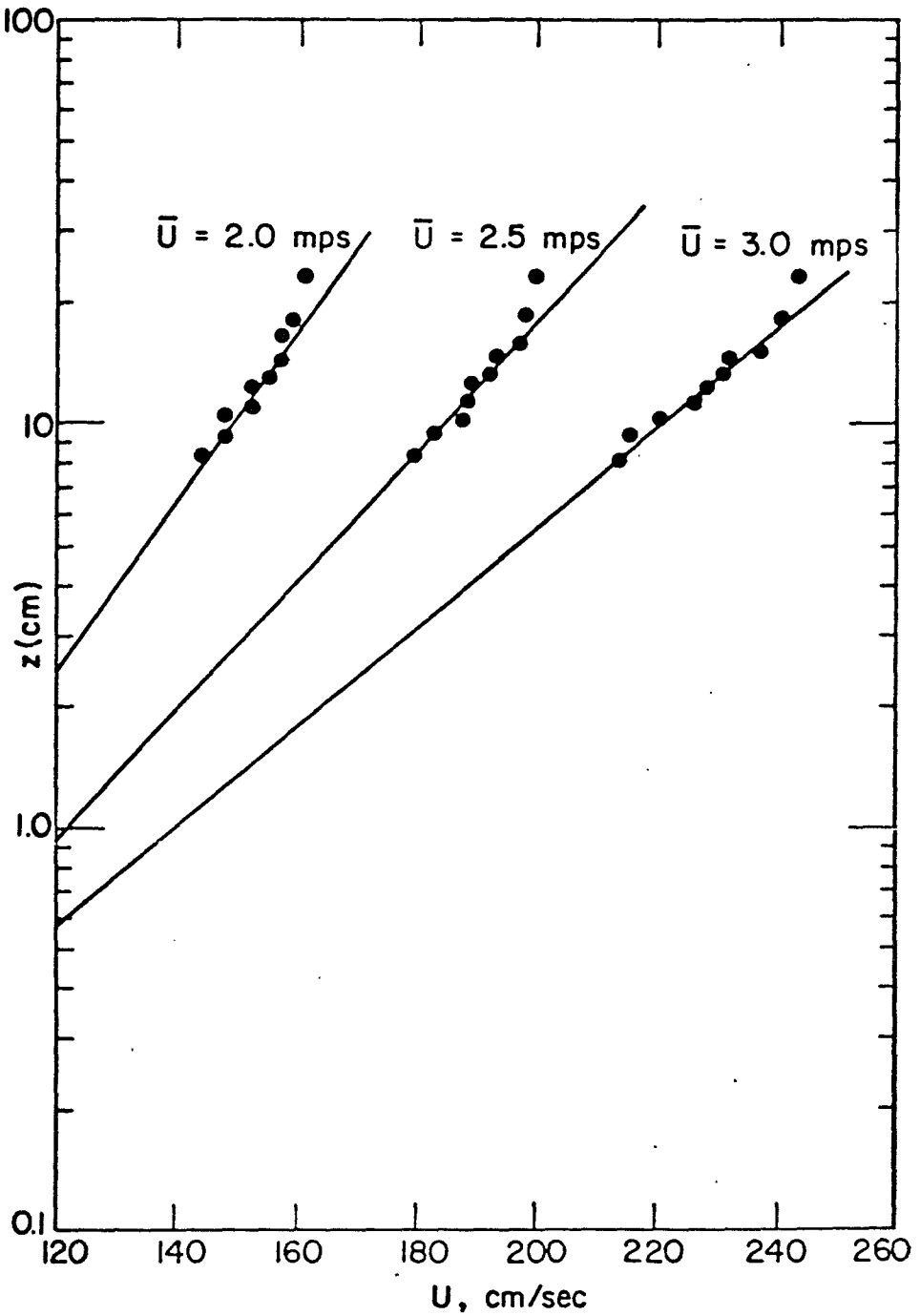

Figure 37. Wind velocity vs. log z, (height z) above SWL.

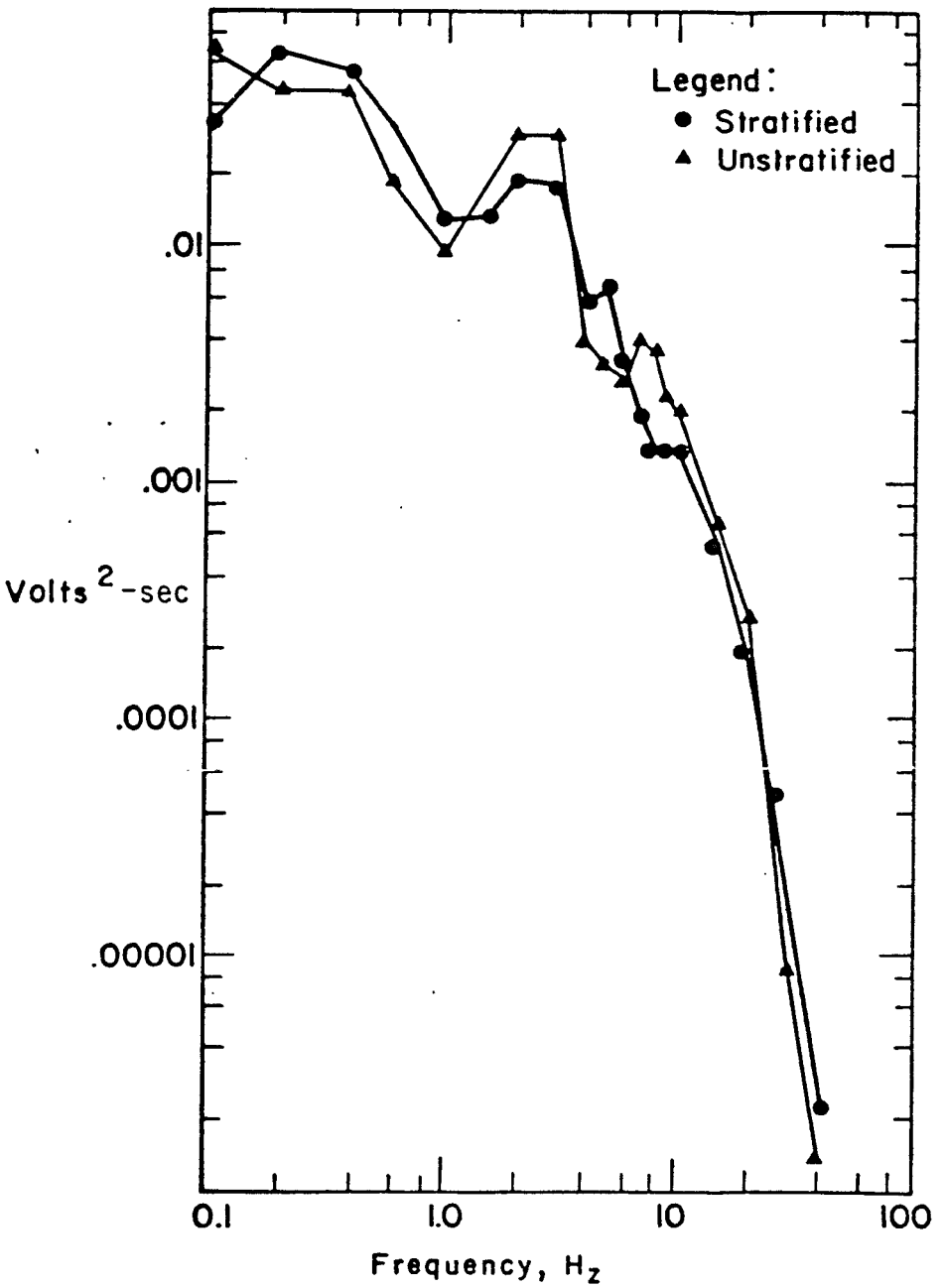

Figure 38. One dimensional scalar energy spectra at a depth of 2 cm.

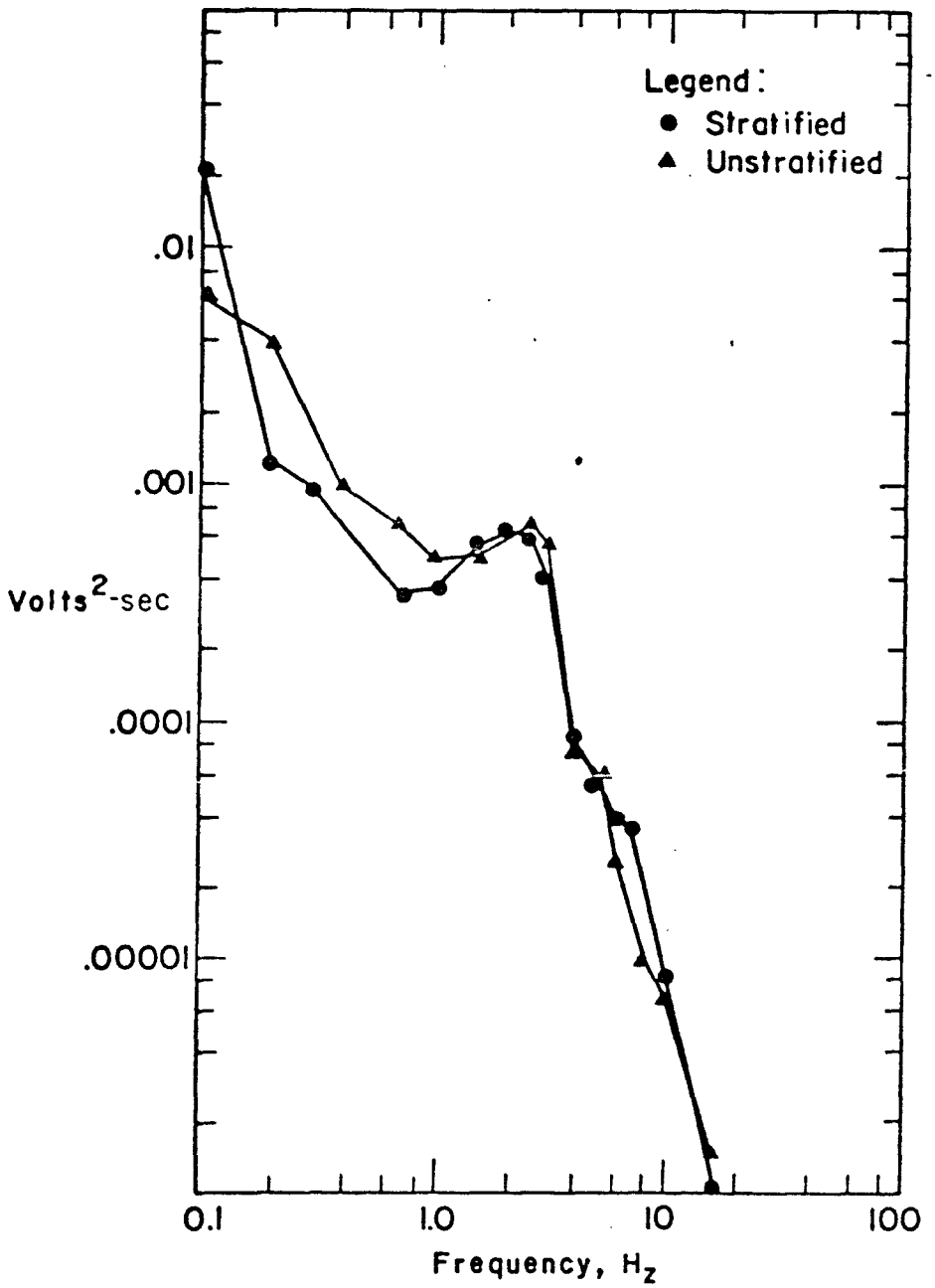

Figure 39. One dimensional scalar energy spectra at a depth of 10 cm.

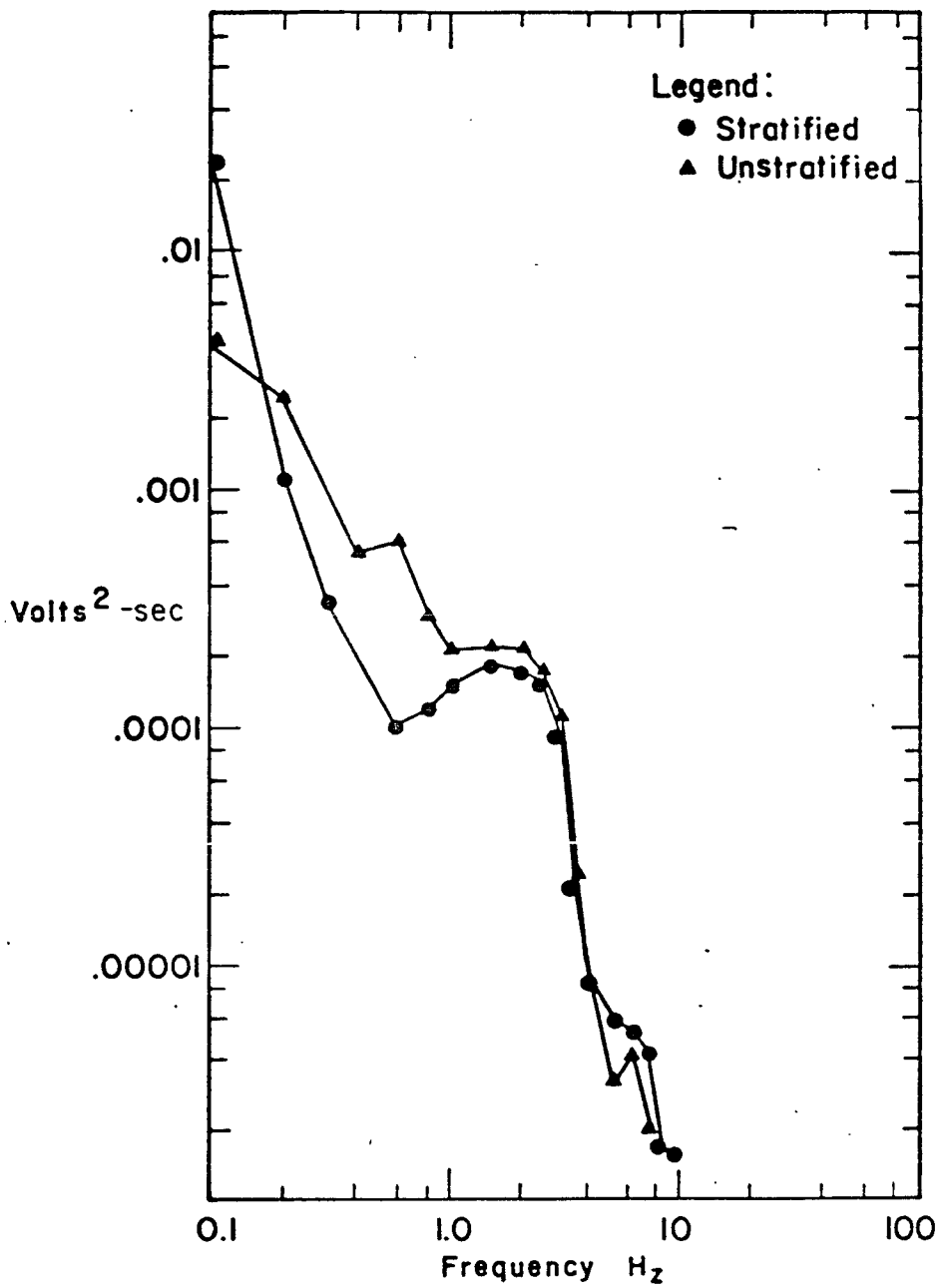

Figure 40. One dimensional scalar energy spectra at a depth of 15 cm.

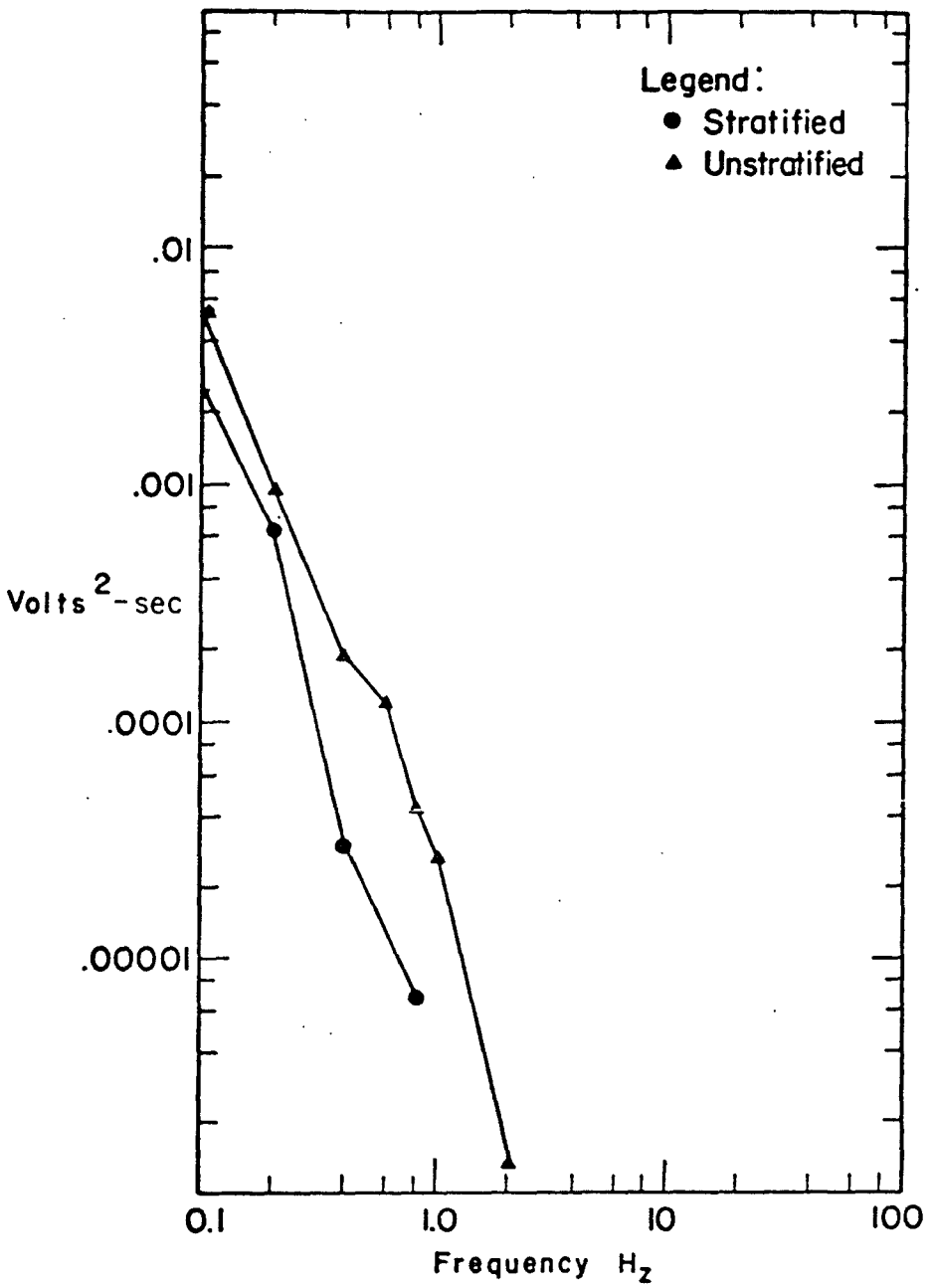

Figure 41. One dimensional scalar energy spectra at a depth of 33 cm.

energy between the stratified and unstratified situations at the same depth. The position of the interface during the recording of the turbulence was just below 33 cm, a depth which develops after 1 hour of wind at 2.5 mps. The bandwidth for the analysis was .1 Hz for the range .1 Hz to 1 Hz, 1 Hz for the range 1 to 10, and 10 Hz for the range 10 Hz to 100 Hz. For 80% confidence the results in each of these three ranges were within 70%, 20%, and 10% of the true values, respectively (Schiesser).

V. DISCUSSION OF RESULTS

In the initial phase of experimentation the density profiles (Figures 7-31) lend themselves to examination by continuity. If the original profile is integrated to give the mass of a column of water of unit surface area, the result should be the same for the profile under wind. This was found to be untrue; in general the integral of the density profile at the downwind end of the tank is less than that of the initial profile, while at the upwind end it is greater. Figures 32 and 33 illustrate the density structure with an internal setup due to the wind stress. Determination of rate of entrainment is thus complicated by the internal setup and return flow.

The shear velocity above the interface at the downwind end of the tank might normally be expected to be higher than at the upwind end due to the boundary conditions of a tank of finite length. However, the greater potential energy of the buoyancy field at the upwind end of the tank presents an unstable situation which results in a counter current driven by buoyancy forces. Figure 42 illustrates the varied velocity profiles which occur along the length of the tank. This figure was drawn from observations of the movements of particles suspended in the water. It is not a steady state situation because of the constantly changing buoyancy forces, but it is typical. Unfortunately not enough velocity measurements were made to verify this, but making the assumption that the velocity gradients at the interface are of the same order of magnitude along the length of the tank results in a Richardson number at the down-

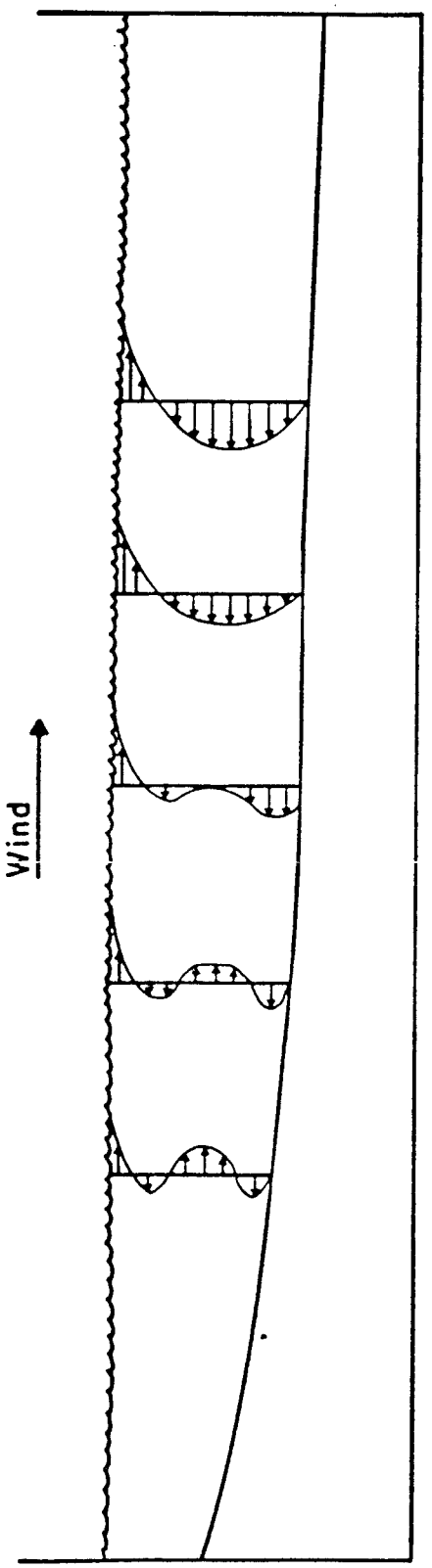

Figure 42. Velocity distributions induced by wind over a closed basin with a stable stratification.

wind end of the tank about 500 times greater than at the upwind end. In addition the relative shallowness of the interface and smaller density jump across it at the upwind end would increase the entrainment coefficient of Kato and Phillips. From this it is hypothesized that the majority of mixing takes place very near the upwind end of the tank. The evidence is by no means conclusive, but the Richardson numbers calculated from the velocity data taken in the second phase of experimentation support this hypothesis.

The overall Richardson number 16 meters from the upwind end of the tank was 200 with the interface at a depth of 33 cm, 4 hours later it was 267 with the interface at 36 cm. The shear velocity term in the overall Richardson number was determined from Figure 37 and

$$u_{*_w} = (\rho_a \, u_{*a}^2/\rho_w)^{\frac{1}{2}} .$$

The interface receeded 3 cm in the 4 hours between the recording of velocity profiles giving an experimental $\bar{u}_e$ of 2.1×10^{-4} cm/sec. The relationship found by Kato and Phillips predicts $\bar{u}_e = 1.1 \times 10^{-2}$ cm/sec.

Some differences between the results of Kato and Phillips are to be expected due to the differences in the scale of the experiments but the same parameters are used in defining the Richardson number so this great difference indicates that some other mechanism may be responsible. There are several possibilities which will be discussed but first a word about the quality of the data is in order.

In the first phase of the experiments an attempt was made to reproduce the starting density profile as consistently as possible so that comparisons could be made between the different runs. For a given wind velocity the position of the interface at the end of three, four, and five hours should give an estimate of the average rate of entrainment over two periods of

one hour each. In general this is correct but the quantitative aspects of the entrainment rate is poor due to slight variations in the slope of the linear approximation to the density profile, and perhaps even more significant is the variation in curvature. For example, considering the density profiles at station 18 for a wind velocity of 3 mps (Figures 29, 30, and 31), a greater entrainment velocity is indicated from 4 to 5 hours than from 3 to 4 hours. Due to the increasing density gradient and depth of the interface with time, this should not be so according to the expression for the entrainment constant. A close look at the initial profiles reveals that the 5 hour case had a gradual curvature concave upwards while the other two were less curved and exhibited concavity both up and down at different levels. Mixing of a finite element of a fluid with a profile concave upward will result in positive buoyancy for that element (Long, 1970), consequently, it will rise into the turbulent region and be completely mixed with the upper layer and produce a lowering of the interface. The same element in a fluid with the concavity of the profile downwards would have a negative buoyancy and sink back towards the interface rather than being immediately mixed with the turbulent layer, thereby slowing the entrainment. This in itself is an interesting observation, but the presence of this anomaly makes it difficult to determine an entrainment constant from the data.

In addition to the relative magnitudes of the entrainment in the two experiments, there is a non-uniformity in the entrainment velocity along the length of the tank. An expression for the entrainment might look like

$$E(R_i, x) = f(x) \frac{\rho_o u_{*w}^2}{g\delta\rho D} \quad , \qquad (5)$$

where ρ_0 is the mixed layer density and

$$f(x) = \frac{l-x}{l} \quad , \tag{6}$$

where l is the length of the tank and x is the horizontal distance from the upwind end of the tank. It does not matter that f(x) vanished at x=l since at the boundary u_* also becomes zero. The resulting form of the entrainment constant is

$$E(R_i, x) = C \frac{l-x}{l} \frac{\rho_o u_{*w}^2}{g\delta\rho D} \quad , \tag{7}$$

where the proportionality constant c must be determined empirically from a plot of the experimentally observed entrainment velocity vs. $(\frac{l-x}{l}) \frac{\rho u_*^3}{g\delta\rho D}$. A plot of the data from the first phase of experimentation, after eliminating some of the obviously bad data points and averaging the entrainment velocities, results in a least squares fit to a straight line with a slope of .108 as shown in Figure 43. Equation (7) becomes

$$E(R_i, x) = .108 \left(\frac{l-x}{l}\right) \frac{\rho_o u_{*w}^2}{g\delta\rho D} \quad . \tag{8}$$

Application of this to the second phase of experimentation results in a prediction of u_e = .000198 with the interface at a depth of 35 cm, as compared with a value of .00021 experimentally, averaged over the whole 4 hour run. The agreement is not so good over the earlier and latter parts of the run where the experimental values are respectively higher and lower than the predictions. The initial density profile shows some curvature which would effect entrainment as mentioned earlier. Since negative curvature increases entrainment and positive curvature retards it, the entrainment constant might be modified to include a curvature term K, and Equation (8) may assume the form

$$E(R_i, x, K) = .108 \left(\frac{l-x}{l}\right) \frac{\rho_o u_{*w}}{g\delta\rho D} (1-K^a) \quad , \tag{9}$$

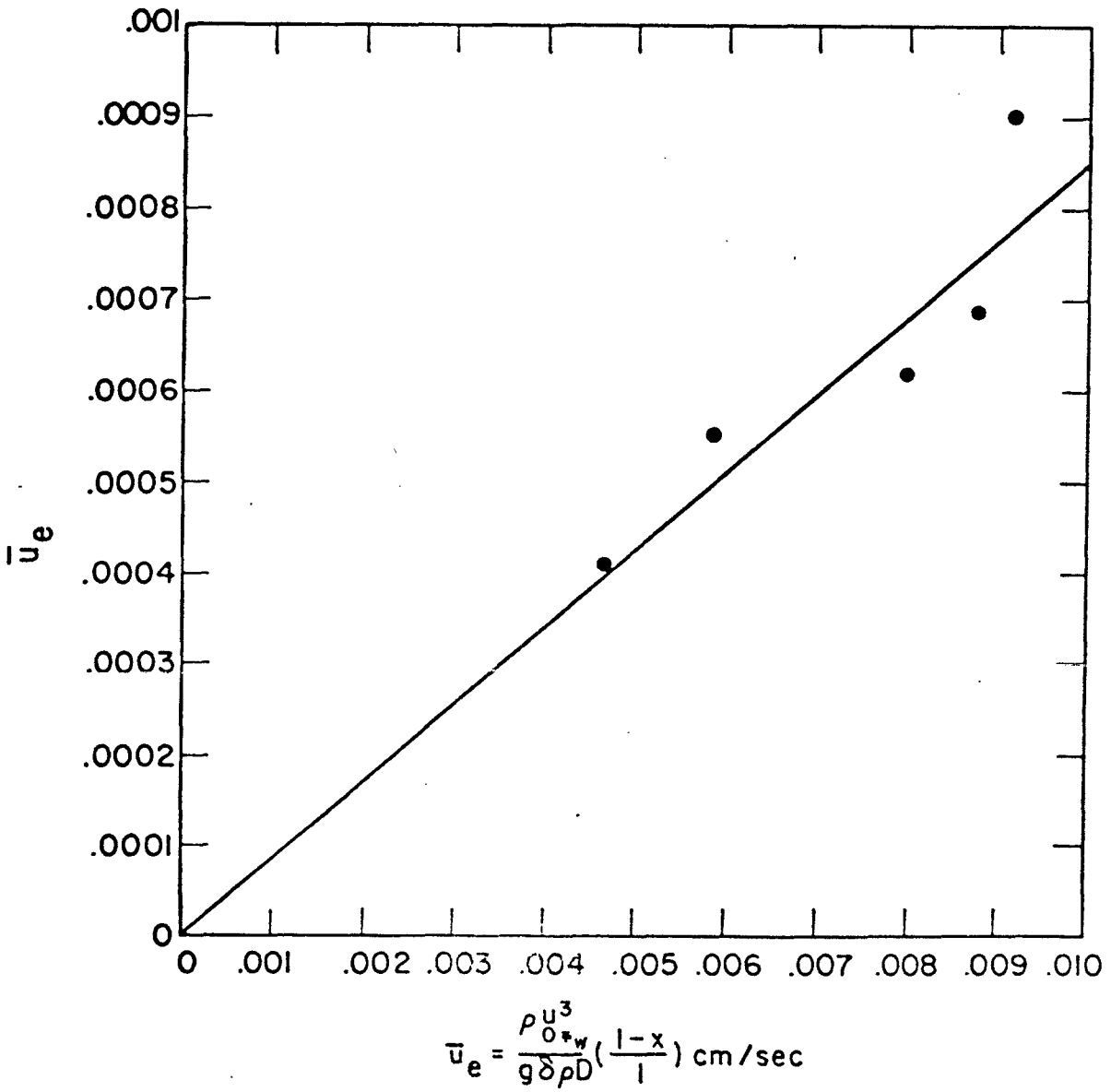

Figure 43. Experimentally observed entrainment velocity vs. predicted entrainment velocity.

where a is a constant. Since a very small curvature has a pronounced effect on entrainment, a will be small. Approximating the curvature as circular over a small region and obtaining a radius of curvature $R = \frac{1}{K}$ from the initial profile it is estimated, $a \simeq .03$.

The range of eddy sizes supporting the Reynolds stresses is the same as that containing the bulk of the kinetic energy of the turbulence. From the spectra it is obvious that the stable stratification reduces the transfer of energy to the large scale turbulence, as predicted by Phillips hypothesis by reducing the Reynolds stress. The small scale turbulence, i.e. the equilibrium and dissipation range is at a much higher frequency than the $N = \sqrt{\frac{g}{\rho}\frac{\partial \rho}{\partial z}}$ for the upper layer, which would be in the neighborhood of .1 sec^{-1}. Near the interface, $N \simeq 1$ and a corresponding reduction in turbulence in this range is observed just above the interface.

It would be useful to compare these turbulent energy spectra to the corresponding situation with no return flow. With return flow for the same surface shear there would be a larger horizontal velocity gradient in the vertical direction which would increase viscous dissipation. There must also be a level at which $\frac{\partial u}{\partial z} = 0$, which would inhibit the energy transfer by Reynolds stresses. Considering these two factors we would expect a lower level of turbulent energy near the interface when a return flow is present, and therefore a lower rate of entrainment.

Besides these two reasons for expecting slower entrainment with return flow, there are also surface and internal setups and the shear stresses required to maintain those setups. The viscous forces would contribute to the energy dissipation term. The internal setup represents a transfer of kinetic energy to potential energy within the system, but

VI. CONCLUSIONS AND RECOMMENDATIONS

The functional relationship between the overall Richardson number and the entrainment is verified but additional factors must be considered when the applied shear stress is a function of the distance along the surface of applied shear, and a return flow is present. The mechanism by which return flow modifies the entrainment is due to the shear flow at the interface and the mean shear flow in the turbulent layer with its associated effect on the Reynolds stresses. Due to the density structure of the internal setup, buoyancy forces play an additional role not seen in the situation with no return flow, and considerations of curvature in the initial density profile indicate that buoyancy effects are very important when the initial profile is not linear.

The first recommendation is that in future research in this area, less time should be spent measuring initial and final density profiles, and more effort go into studying the dynamic situation. More accurate measurement of entrainment rates is needed to substantiate the empirical results presented here. The same is true for the entrainment constant involving the curvature term, although for what was originally intended as the object of this study it would have been better if a better method for establishing and reproducing linear density profiles had been available, leaving the curvature effects to be studied separately.

Perfection of the conductivity probe and the associated electronics would facilitate the collection of density data. The method used here for measuring density profiles was so time consuming that the profile would change during the time required for measurement, thus introducing an additional source of error.

The effects of stratification on turbulent energy transfer are verified in that the one dimensional scalar energy spectra presented here show a greater decrease in turbulent energy over depth for the stratified case. The development of the theory behind this depends on the correlation of the vertical velocity fluctuations at two separate points so that a quantitative discussion would need such measurements. Determination of the scalar energy spectrum (Equation (2)) also requires turbulence measurements from two points with separation r, so it is recommended that additional studies in this area should include measurement of at least two fluctuating components at two separate points. These measurements would eliminate the need for the isotropic assumption, and along with the information which could be gathered with two conductivity probes it would be possible to determine the net local buoyancy flux.

is unlike the potential energy increase due to entrainment in that it is recoverable, and manifests itself in the form of an internal seiche when the surface shear is removed.

APPENDIX A

DIFFUSIVITY OF NaCl IN WATER

The assumptions were made that molecular diffusion and salinity increase from evaporation were insignificant compared to turbulent mixing and overall salinity. The mass transfer due to molecular diffusion is given by

$$N_A = \frac{D_{AB}}{ZX_{BM}} \left(\frac{\rho}{M}\right) (X_{A1} - X_{A2})$$

N_A = Mass flux of salt

D_{AB} = Molecular diffusivity

Z = Thickness of diffusion layer

$$X_{BM} = \frac{X_{B1} - X_{B2}}{\ln(X_{B2}/X_{B1})}$$

X_{A1}, X_{A2}, X_{B1}, X_{B2} = Mole fractions of salt and water in the salt and fresh water layers, respectively

ρ = Density of salt water

M = Molar weight of salt water.

An exaggerated estimate of the diffusion can be given by assuming $X_{A2} = 0$, therefore $X_{B2} = 1$ and $D_{AB} = 1.3 \times 10^{-5}$ cm^2/sec (Treyball, 1968) which results in

$$N_A = \frac{1.3 \times 10^{-5} \text{ cm}^2/\text{sec}}{(.1 \text{ cm})(3.1)} \left(.056 \frac{\text{g mole}}{\text{cm}^3}\right) (.009) \left(\frac{5.3 \text{ g}}{\text{g mole}}\right)$$

$$= 1.113 \times 10^{-6} \text{ g/cm}^2/\text{sec} \quad .$$

As a comparison, a 1 cm erosion of the interface across which $c = .03$ g/cm would result in the transfer of .03 g of salt to the upper layer, the ratio of this to the transport due to diffusion over one hour is approximately 10. In the experiment the salinity jump across the interface is less than for the above calculated diffusion, it is therefore safe to say that molecular diffusion is at the very most one order of magnitude smaller than the turbulent diffusion, and may be neglected.

APPENDIX B

NEGATIVE BUOYANCY GENERATION AT THE SURFACE DUE TO EVAPORATION

Mass transfer per unit area between a flat gas-liquid interface is given by (Treyball, 1968)

$$N_A M_A = M_A F_G \left(\ln \frac{1 - P_{Ai}/p_t}{1 - P_{AG}/p_t}\right) \qquad (B1)$$

where

N_A = Molar flux

M_A = Molecular wt = 18 lb/lb mole

F_G = Mass transfer coefficient

P_{Ai} = Vapor pressure of the liquid (A) at the interface = 17.535 mm Hg

P_{AG} = Partial pressure of the liquid in the gas

p_t = Total pressure = 760 mm Hg.

The mass transfer coefficient is obtained by the heat-mass transfer analogy with the empirical relationship (Treyball, 1968)

$$h = 0.072\ G'^{0.6}$$

where h is the heat transfer coefficient between an air water interface and G' is a superficial air mass velocity. The heat transfer dimensionless group defined by

$$j_H = \frac{h}{C_p U \rho} P_r^{2/3} \qquad (B2)$$

c_p = Heat capacity of gas

U = Velocity of gas

ρ = Density of gas

P_r = Dimensionless Pradtl number = $\frac{C_p x \text{ viscosity}}{\text{thermal conductivity}}$

can be related by the heat-mass transfer analogy to the mass transfer dimensionless group

$$j_D = \frac{k_G P_{BM} M}{\rho U} S_c^{2/3} \qquad (B3)$$

where

K_G = Mass transfer coefficient per concentration difference

P_{BM} = Log mean partial pressure difference

M = Molecular weight of the gas

S_c = The dimensionless Schmidt number

$$= \frac{\text{Kinematic viscosity}}{\text{Diffusivity of water vapor in air}} .$$

Equating (B2) and (B3)

$$\frac{h}{C_p U \rho} P_r^{2/3} = \frac{K_G P_{BM} M}{\rho U} S_c^{2/3} .$$

The mass transfer coefficient F_G is determined,

$$F_G = K_G P_{BM} = \frac{h}{C_p G} P_r^{2/3} \frac{\rho U}{M} S_c^{2/3} .$$

For air at 5 fps the value of F_G is .0114 lb mile/hr ft^2. Substituting this into (B1) and making the extremely exaggerated assumption that the air is initially at zero humidity, the evaporation after one hour would be

.0023 grams H_2O/cm^2. This would leave behind

$$\left(\frac{.0023\ gH_2O}{cm^2\ hr}\right)\left(\frac{.006\ gNaCl}{g\ H_2O}\right) = 1.38 \times 10^{-5}\ g\frac{NaCl}{cm^2} \quad ,$$

when the top layer is at a concentration of .006 g $NaCl/gH_2O$ as in the experiment. The ratio of the amount of salt left behind to the concentration in solution is 2×10^{-4}; evaporation can therefore be neglected.

BIBLIOGRAPHY

Ellison and Turner, 1959, "Turbulent Entrainment in Stratified Fluids," Journal of Fluid Mechanics, Vol. 6, pp. 423-448.

Gibson, C. H. and Schwarz, W. H., 1963, "Detection of Conductivity Fluctuations in a Turbulent Flow Field," Journal of Fluid Mechanics, Vol. 16, pp. 357-364.

Kato and Phillips, 1969, "On the Penetration of a Turbulent Layer into a Stratified Fluid," Journal of Fluid Mechanics, Vol. 37, pp. 643-655.

Long, R. R., 1970, "A Theory of Turbulence in Stratified Fluids," Journal of Fluid Mechanics, Vol. 42, pp. 349-365.

Morton, B. R., Taylor, Sir Goeffrey, and Turner, J. S., 1956, Proceedings of the Royal Society of London, Series A, Vol. 234, Jan. 24 - Mar. 6.

Phillips, 1969, The Dynamics of the Upper Ocean, Cambridge University Press.

Schiesser, W. E., Statistical Uncertainty of Power Spectral Estimates.

Shemdin, O. H., 1972, "Wind-Generated Current and Phase Speed of Wind Waves," Journal of Physical Oceanography, Vol. 2, No. 4.

Sheppard, D. M., Shemdin, O. H., and Wang, Y. H., 1973, "A Multipurpose Internal Wave Facility," Technical Report No. 19, Coastal and Oceanographic Engineering Laboratory, University of Florida, June.

Tennekes, H. and Lumley, J. L., 1972, A First Course in Turbulence, MIT Press.

Treyball, R. E., 1968, Mass Transfer Operations, McGraw-Hill Book Co.

Turner, 1968, "The Influence of Molecular Diffusivity on Turbulent Entrainment Across a Density Interface," Journal of Fluid Mechanics, Vol. 33, pp. 639-656.